Estimating the Uncertainty on J/ψ Production

R. Vogt (LLNL and UC Davis)

Outline

- **Production in pp – Color Evaporation**
- **Fraction of J/ψ from B Decays**
- **Brief Discussion of Cold Matter Effects**

Color Evaporation

All quarkonium states are treated like $Q\overline{Q}$ ($Q = c, b$) below $H\overline{H}$ ($H = D, B$) threshold

Distributions for all quarkonium family members similar, modulo decay feed down, production ratios should be independent of $\sqrt{s}$

At LO, $gg \to Q\overline{Q}$ and $q\overline{q} \to Q\overline{Q}$; NLO add $gq \to Q\overline{Q}q$

$$\sigma_Q^{\rm CEM} = F_Q \sum_{i,j} \int_{4m_Q^2}^{4m_H^2} d\hat{s} \int dx_1 dx_2 \; f_{i/p}(x_1, \mu^2) \; f_{j/p}(x_2, \mu^2) \; \hat{\sigma}_{ij}(\hat{s}) \; \delta(\hat{s} - x_1 x_2 s)$$

Values of m_Q and Q^2 fixed from NLO calculation of $Q\overline{Q}$ production

Main uncertainties arise from choice of PDFs, heavy quark mass, renormalization (α_s) and factorization (evolution of PDFs) scales

Inclusive F_Q fixed by comparison of NLO calculation of $\sigma_Q^{\rm CEM}$ to $\sqrt{s}$ dependence of J/ψ and Υ cross sections, $\sigma(x_F > 0)$ and $Bd\sigma/dy|_{y=0}$ for J/ψ, $Bd\sigma/dy|_{y=0}$ for Υ

Data and branching ratios used to separate the F_Q's for each quarkonium state

Resonance	J/ψ	ψ'	χ_{c1}	χ_{c2}	Υ	Υ'	Υ''	$\chi_b(1P)$	$\chi_b(2P)$
$\sigma_i^{\rm dir}/\sigma_H$	**0.62**	**0.14**	**0.6**	**0.99**	**0.52**	**0.33**	**0.20**	**1.08**	**0.84**
f_i	**0.62**	**0.08**	**0.16**	**0.14**	**0.52**	**0.10**	**0.02**	**0.26**	**0.10**

Table 1: **The ratios of the direct quarkonium production cross sections, $\sigma_i^{\rm dir}$, to the inclusive J/ψ and Υ cross sections, denoted σ_H, and the feed down contributions of all states to the J/ψ and Υ cross sections, f_i, Digal *et al.*.**

Why Still CEM?

Open and hidden charm photo- and hadroproduction show similar energy dependence

High p_T Tevatron Run I data show that, within uncertainties of the data, the prompt J/ψ, the ψ' and χ_c p_T dependencies are the same

Amundsen *et al.* calculated p_T distribution (only partial real part) harder than data at high p_T, undershoots at low p_T – likely because they do not include any k_T smearing

Gavai *et al.* calculated complete J/ψ p_T distribution starting from exclusive NLO $Q\overline{Q}$ production code by Mangano *et al.*

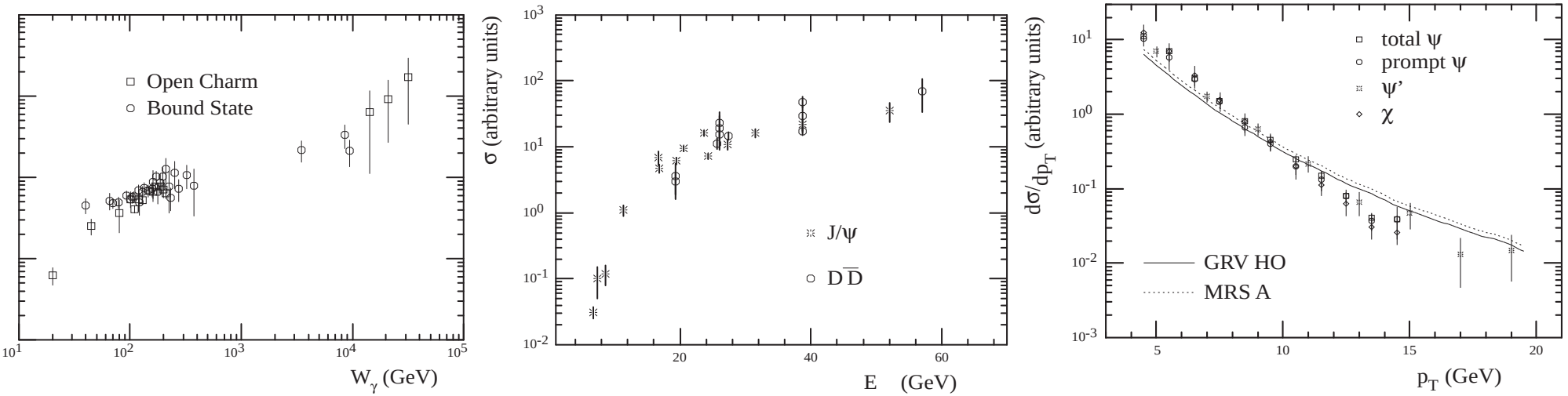

Figure 1: **(Left) Photoproduction data as a function of the photon energy in the hadron rest frame, W_γ. (Center) Hadroproduction data as a function of the center-of-mass energy, E_{cm}. In both cases, the normalization has been adjusted to show the similar shapes of the data. (Right) Run I data from the CDF Collaboration, shown with arbitrary normalization. The curves are the predictions of the color evaporation model at tree level, also shown with arbitrary normalization. [Amundson *et al.*]**

How to Fix the Uncertainty on the CEM Result?

Previously took 'by eye' fit to $Q\overline{Q}$ total cross section

Dates back to original Hard Probes Collaboration report in 1995 – only PDF changed over time

Since I've been asked what the uncertainty on the cross section is, I have to try to invent some, work in progress

Choosing J/ψ Parameters I: FONLL-based

Main sources of uncertainty:

Mass: $1.3 < m < 1.7$ **GeV for charm (central value, 1.5 GeV)**

Scale: renormalization, μ_R**, and factorization,** μ_F**, scales governing** α_s **and PDF behavior respectively**

Parton Density: evolution of gluon density

With a given PDF set define a fiducial region of mass and scale that should encompass the true value:

- **For** $\mu_F = \mu_R = m$**, vary mass between upper and lower end of range;**
- **For central mass value, vary scales independently within a factor of two:** $(\mu_F/m, \mu_R/m) = (1,1)$**, (2,2), (0.5,0.5), (0.5,1), (1,0.5), (1,2), (2,1).**

Define upper and lower bounds of theoretical values; the maximum and minimum may not come from the same set of parameters at a given energy or p_T

The uncertainty band comes from the upper and lower limits of mass and scale uncertainties added in quadrature:

$$\sigma_{\max} = \sigma_{\text{cent}} + \sqrt{(\sigma_{\mu,\max} - \sigma_{\text{cent}})^2 + (\sigma_{m,\max} - \sigma_{\text{cent}})^2}$$

$$\sigma_{\min} = \sigma_{\text{cent}} - \sqrt{(\sigma_{\mu,\min} - \sigma_{\text{cent}})^2 + (\sigma_{m,\min} - \sigma_{\text{cent}})^2}$$

FONLL Calculation of $c\bar{c}$ Uncertainty

$c\bar{c}$ cross section dependence on $\sqrt{s}$ with FONLL parameter sets (left), uncertainty band on $c\bar{c}$ cross section (right)

None of the FONLL sets fit the data, large χ^2/dof

No convergence for $\mu_R/m < 1$ (large α_s)

Problems with backward evolution of PDFs for $\mu_F/m \leq 1$ (near or below minimum scale of PDFs)

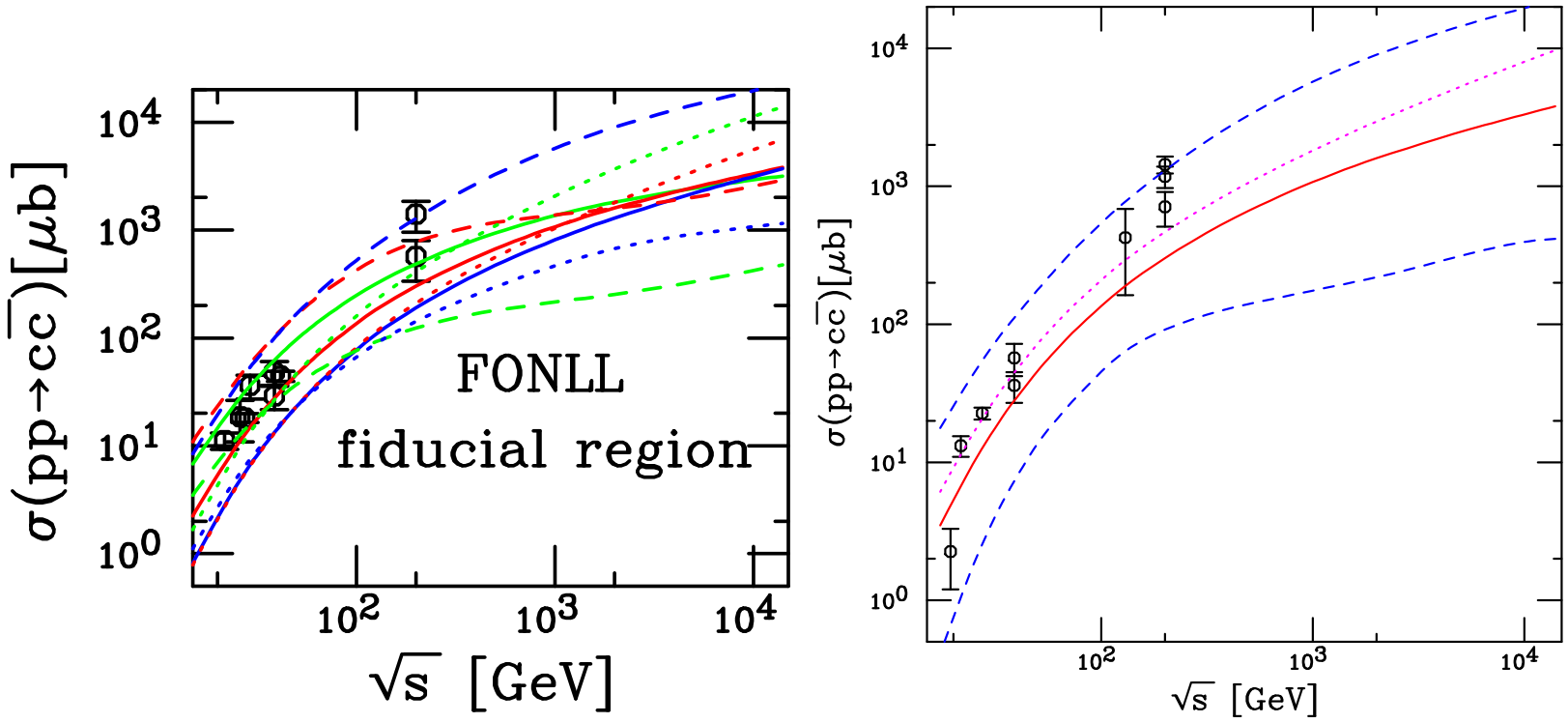

Figure 2: (Left) Total $c\bar{c}$ cross sections calculated using CTEQ6M. The solid red curve is the central value $(m, \mu_F/m, \mu_R/m) = (1.5\,\text{GeV}, 1, 1)$. The green and blue solid curves are $(1.3\,\text{GeV}, 1, 1)$ and $(1.7\,\text{GeV}, 1, 1)$ respectively. The red, blue and green dashed curves correspond to $(1.5\,\text{GeV}, 0.5, 0.5)$, $(1.5\,\text{GeV}, 1, 0.5)$ and $(1.5\,\text{GeV}, 0.5, 1)$ while the red, blue and green dotted curves are for $(1.5\,\text{GeV}, 2, 2)$, $(1.5\,\text{GeV}, 1, 2)$ and $(1.5\,\text{GeV}, 2, 1)$. (Right) Uncertainty band formed from adding mass and scale uncertainties in quadrature.

J/ψ Uncertainty Large, Can Only Define Upper Limit

Fit F_C CEM parameter for central mass and scale value, use same value for other calculations of fiducial range

At large $\sqrt{s}$ $(\mu_F/m, \mu_R/m) = (0.5, 0.5)$, (0.5,1) flattens because $\mu_F < \mu_0$ of PDF

$m_c = 1.7$ GeV governs uncertainty at low $\sqrt{s}$ since $m_D/m_c \sim 1.1$, small phase space for J/ψ production in CEM – doesn't make much sense

Large combination of mass and scale uncertainty makes lower limit ill defined

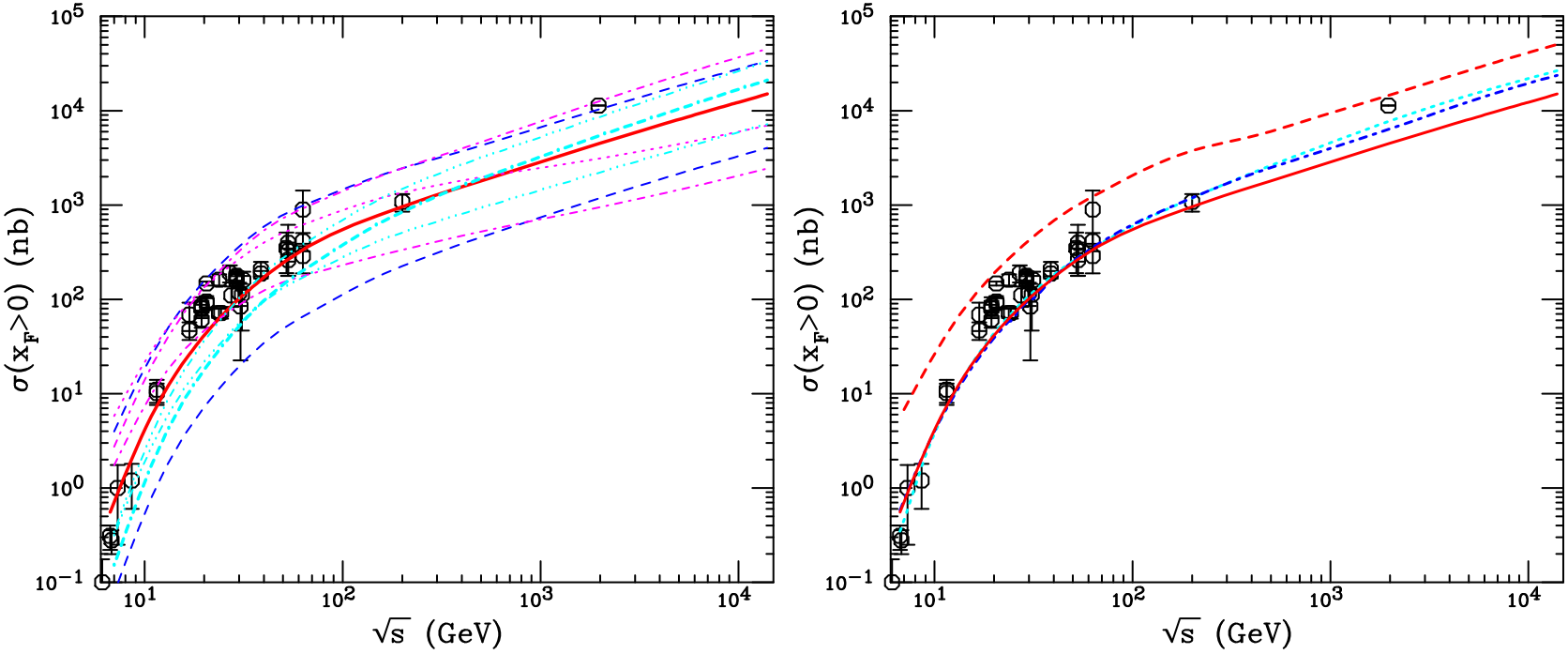

Figure 3: **(Left) Total J/ψ cross sections calculated using CTEQ6M. The solid red curve is the central value $(\mu_F/m, \mu_R/m) = (1, 1)$ with $m = 1.5$ GeV. The upper and lower dashed blue curves are $m = 1.3$ and 1.7 GeV with (1,1) respectively. The dotted magenta curve corresponds to (0.5,0.5) while the upper and lower magenta dot-dashed curves (above $\sqrt{s} = 50$ GeV) correspond to (1,0.5) and (0.5,1). The dash-dash-dotted cyan curve curresponds to (2,2) while the upper and lower cyan dot-dot-dot-dashed curves (above $\sqrt{s} = 50$ GeV) are (2,1) and (1,2). The last 6 curves are all calculated for $m_c = 1.5$ GeV. (Right) The solid and dashed red curves are the central value and upper limit for the J/ψ cross section. The solid cyan curve employs the MRST HO distributions while the dot-dashed blue curve is a result with CTEQ6M, both employing $m_c = 1.2$ GeV, $(\mu_F/m_T, \mu_R/m_T) = (2, 2)$.**

Choosing J/ψ Parameters II: Fitting $\sigma_{c\overline{c}}$ (Take 1)

J/ψ parameters based on fits to NLO total $c\overline{c}$ cross section – caveat: full NNLO cross section unknown, could still be large correction

Fix $\mu_F/m = 1, 2$ and let μ_R/m float for range of charm quark masses, $1.1 < m < 1.5$ GeV, used too small quark masses to try to see if a minimum χ^2 has been found – do not go to higher values of m to avoid $m > m_{J/\psi}/2$

$m = 1.27$ GeV is value of charm quark mass from lattice calculations at $m(3\,\mathrm{GeV})$, PDG value, ± 0.9 GeV

Calculate χ^2/dof for fixed-target data alone as well as with RHIC included, check behavior at higher energies, up to LHC

Take best fit values and use these to obtain $c\overline{c}$ cross section below $D\overline{D}$ threshold, find F_c for each mass, scale combination from fit to J/ψ data at $x_F > 0$, extrapolate to LHC energies

Fitting $\sigma_{c\bar{c}}$: Fixed-Target Only

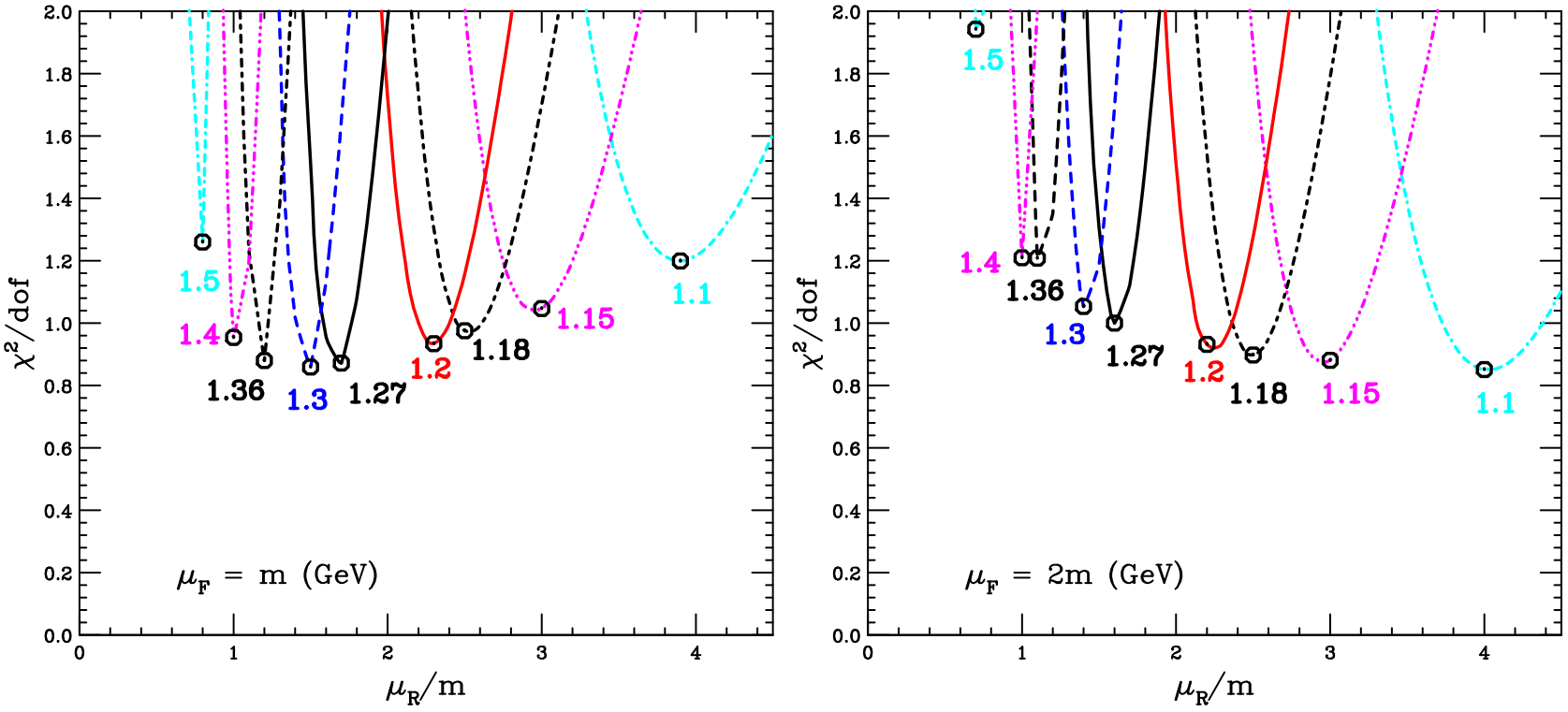

Figure 4: The calculated χ^2/dof for $\mu_F/m = 1$ (left) and 2 (right) at fixed-target energies (excluding RHIC). The circles at the minimum of the curves on the left-hand side correspond to $(1.1\,\text{GeV}, 1, 3.9)$ [dot-dot-dot-dashed black], $(1.15\,\text{GeV}, 1, 3)$ [dot-dash-dash-dashed green], $(1.2\,\text{GeV}, 2, 2.3)$ [solid red], $(1.27\,\text{GeV}, 1, 1.7)$ [dot-dot-dash-dashed black], $(1.3\,\text{GeV}, 1, 1.5)$ [dashed blue], $(1.4\,\text{GeV}, 1, 1)$ [dot-dashed magenta], and $(1.5\text{GeV}, 1, 0.8)$ [dotted cyan] while those on the right-hand side are with $(1.1\,\text{GeV}, 2, 4)$ [dot-dot-dot-dashed black], $(1.15\,\text{GeV}, 2, 3)$ [dot-dash-dash-dashed green], $(1.2\,\text{GeV}, 2, 2.2)$ [solid red], $(1.27\,\text{GeV}, 2, 1.6)$ [dot-dot-dash-dashed black], $(1.3\,\text{GeV}, 2, 1.4)$ [dashed blue], $(1.4\,\text{GeV}, 2, 1)$ [dot-dashed magenta], and $(1.5\text{GeV}, 2, 0.7)$ [dotted cyan]. The calculations are done with the CT10 PDFs.

Fitting $\sigma_{c\bar{c}}$: Including RHIC

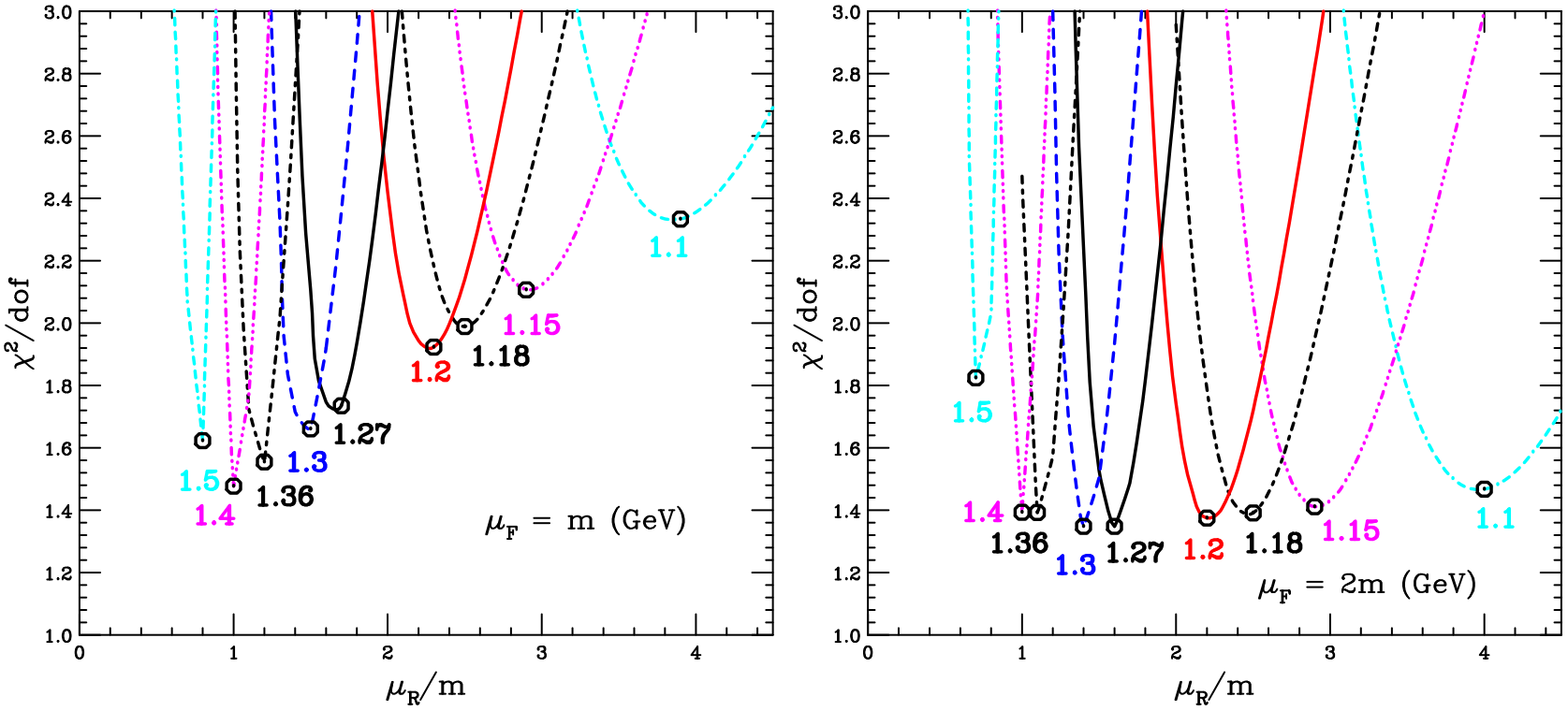

Figure 5: The calculated χ^2/dof for $\mu_F/m = 1$ (left) and 2 (right) including RHIC energies. The circles at the minimum of the curves on the left-hand side correspond to $(1.1\,\text{GeV}, 1, 3.9)$ [dot-dot-dot-dashed black], $(1.15\,\text{GeV}, 1, 3)$ [dot-dash-dash-dashed green], $(1.2\,\text{GeV}, 2, 2.3)$ [solid red], $(1.27\,\text{GeV}, 1, 1.7)$ [dot-dot-dash-dashed black], $(1.3\,\text{GeV}, 1, 1.5)$ [dashed blue], $(1.4\,\text{GeV}, 1, 1)$ [dot-dashed magenta], and $(1.5\text{GeV}, 1, 0.8)$ [dotted cyan] while those on the right-hand side are with $(1.1\,\text{GeV}, 2, 4)$ [dot-dot-dot-dashed black], $(1.15\,\text{GeV}, 2, 3)$ [dot-dash-dash-dashed green], $(1.2\,\text{GeV}, 2, 2.2)$ [solid red], $(1.27\,\text{GeV}, 2, 1.6)$ [dot-dot-dash-dashed black], $(1.3\,\text{GeV}, 2, 1.4)$ [dashed blue], $(1.4\,\text{GeV}, 2, 1)$ [dot-dashed magenta], and $(1.5\text{GeV}, 2, 0.7)$ [dotted cyan]. The locations of the minimum χ^2/dof do not change. The calculations are done with the CT10 PDFs.

Energy Dependence of Best $c\bar{c}$ Fits

Good agreement with fixed-target data does not guarantee good behavior at collider energies

$\mu_F/m = 2$ (right-hand side) gives more realistic $\sqrt{s}$ dependence than $\mu_F/m = 1$ (left-hand side), strongest $\sqrt{s}$ dependence with lowest μ_R/m (0.8) - largest α_s

Low masses flatten cross section for $\sqrt{s} \geq 40$ GeV due to proximity of mass to minimum scale of PDF, especially for $\mu_F = m$

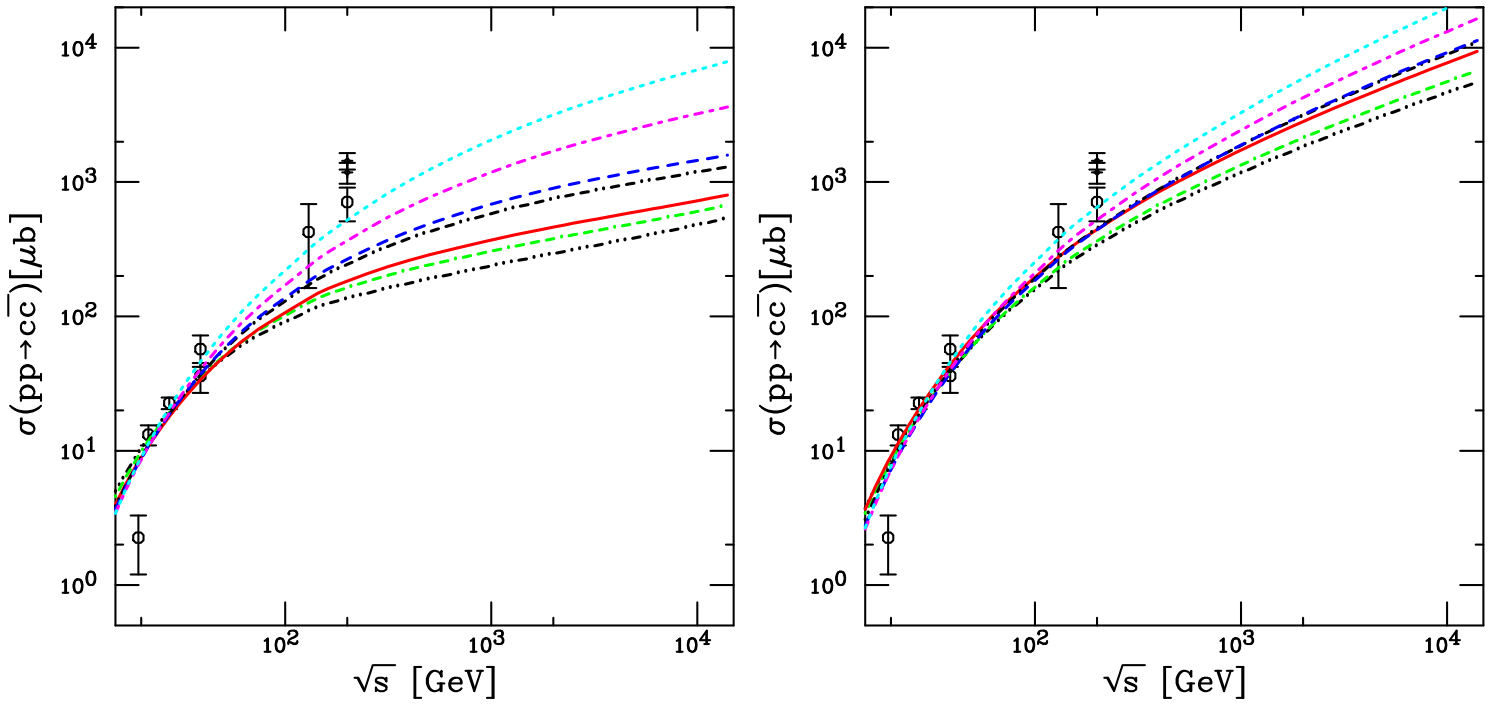

Figure 6: The calculated total $c\bar{c}$ cross sections for $\mu_F/m = 2$ (left) and 1 (right). The circles at the minimum of the curves on the left-hand side correspond to (1.1 GeV, 1, 3.9) [dot-dot-dot-dashed black], (1.15 GeV, 1, 3) [dot-dash-dash-dashed green], (1.2 GeV, 2, 2.3) [solid red], (1.27 GeV, 1, 1.7) [dot-dot-dash-dashed black], (1.3 GeV, 1, 1.5) [dashed blue], (1.4 GeV, 1, 1) [dot-dashed magenta], and (1.5GeV, 1, 0.8) [dotted cyan] while those on the right-hand side are with (1.1 GeV, 2, 4) [dot-dot-dot-dashed black], (1.15 GeV, 2, 3) [dot-dash-dash-dashed green], (1.2 GeV, 2, 2.2) [solid red], (1.27 GeV, 2, 1.6) [dot-dot-dash-dashed black], (1.3 GeV, 2, 1.4) [dashed blue], (1.4 GeV, 2, 1) [dot-dashed magenta], and (1.5GeV, 2, 0.7) [dotted cyan].

J/ψ Cross Sections from $c\overline{c}$ Fits

Take results of $c\overline{c}$ fits, calculate NLO J/ψ cross section in CEM, fit scale factor F_C

Energy dependence almost identical for $\mu_F = 2m_T$, $\sqrt{s}$ dependence generally better

CTEQ6M and CT10 have nearly same value of F_C so previous results compatible with previous results

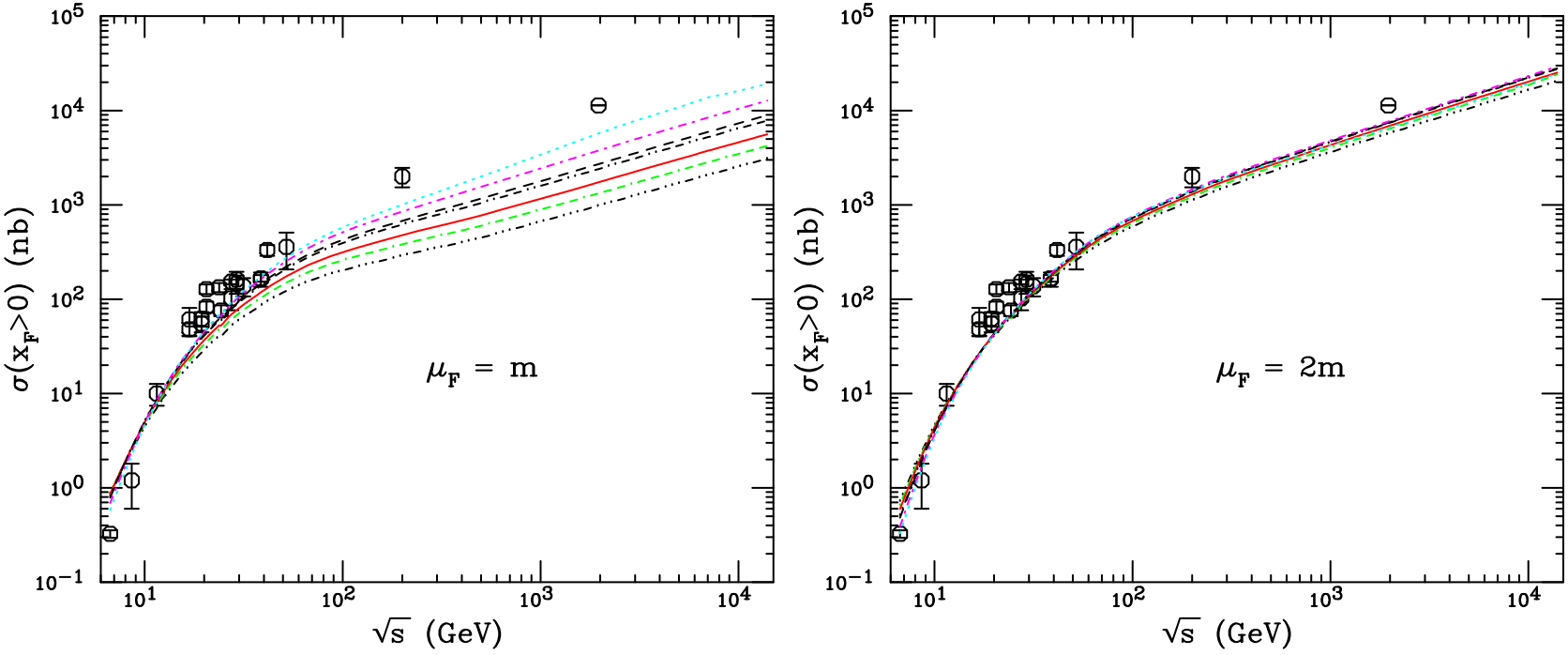

Figure 7: The calculated forward J/ψ cross sections. The curves are calculated with (1.1 GeV, 1, 3.9) [dot-dot-dot-dashed black], (1.15 GeV, 1, 3) [dot-dash-dash-dashed green], (1.2 GeV, 2, 2.3) [solid red], (1.27 GeV, 1, 1.7) [dot-dot-dash-dashed black], (1.3 GeV, 1, 1.5) [dashed blue], (1.4 GeV, 1, 1) [dot-dashed magenta], and (1.5GeV, 1, 0.8) [dotted cyan] while those on the right-hand side are with (1.1 GeV, 2, 4) [dot-dot-dot-dashed black], (1.15 GeV, 2, 3) [dot-dash-dash-dashed green], (1.2 GeV, 2, 2.2) [solid red], (1.27 GeV, 2, 1.6) [dot-dot-dash-dashed black], (1.3 GeV, 2, 1.4) [dashed blue], (1.4 GeV, 2, 1) [dot-dashed magenta], and (1.5GeV, 2, 0.7) [dotted cyan]. (1.2 GeV, 2, 2) [solid red], (1.4 GeV, 2, 1) [dot-dashed magenta], and (1.5 GeV, 2, 0.7) [dotted cyan] using the CT10 PDFs.

Choosing J/ψ Parameters II: Fitting $\sigma_{c\bar{c}}$ (Take II)

No obvious minimum χ^2 region, fits (albeit sometimes lousy ones) can be found for most masses but higher masses require smaller μ_R/m

Broader range of μ_R/m for lower masses but probably unphysically large scales

Location of minimum μ_R/m value does not change much with μ_F/m (see below)

Try to do better by taking PDG value 1.27 ± 0.09 GeV, vary μ_F/m and μ_R/m independently for $1 < \mu/m < 3$, expanding mass range to 3σ around central value and seek to obtain Hessian matrix to get uncertainty – work still in progres

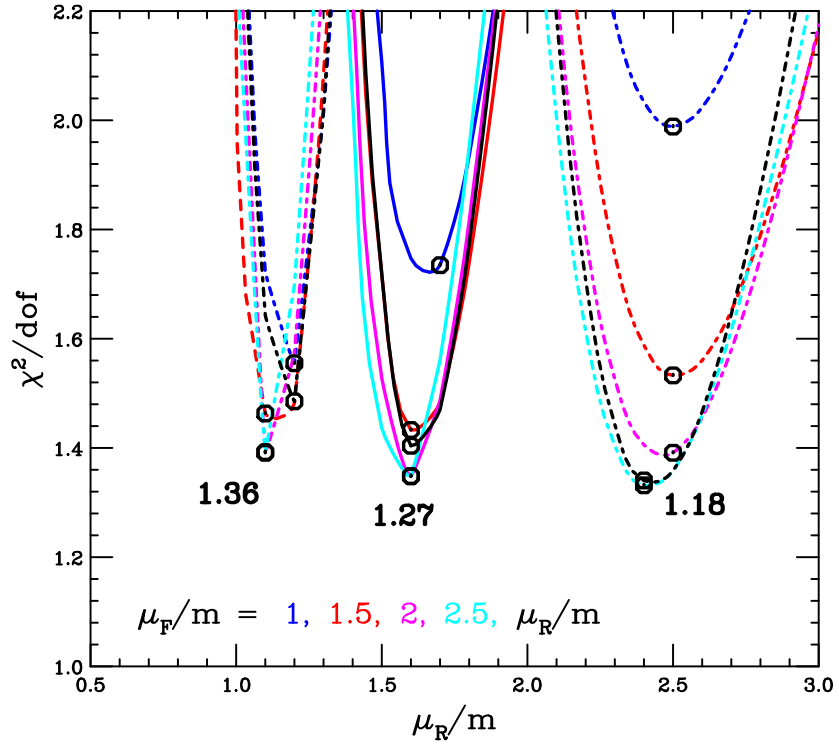

Calculations of $b\bar{b}$ and Υ Better Behaved

Bottom quark mass is large enough for K factors to be smaller and $b\bar{b}$ cross section more reliable
FONLL mass and scale choices work well in this case

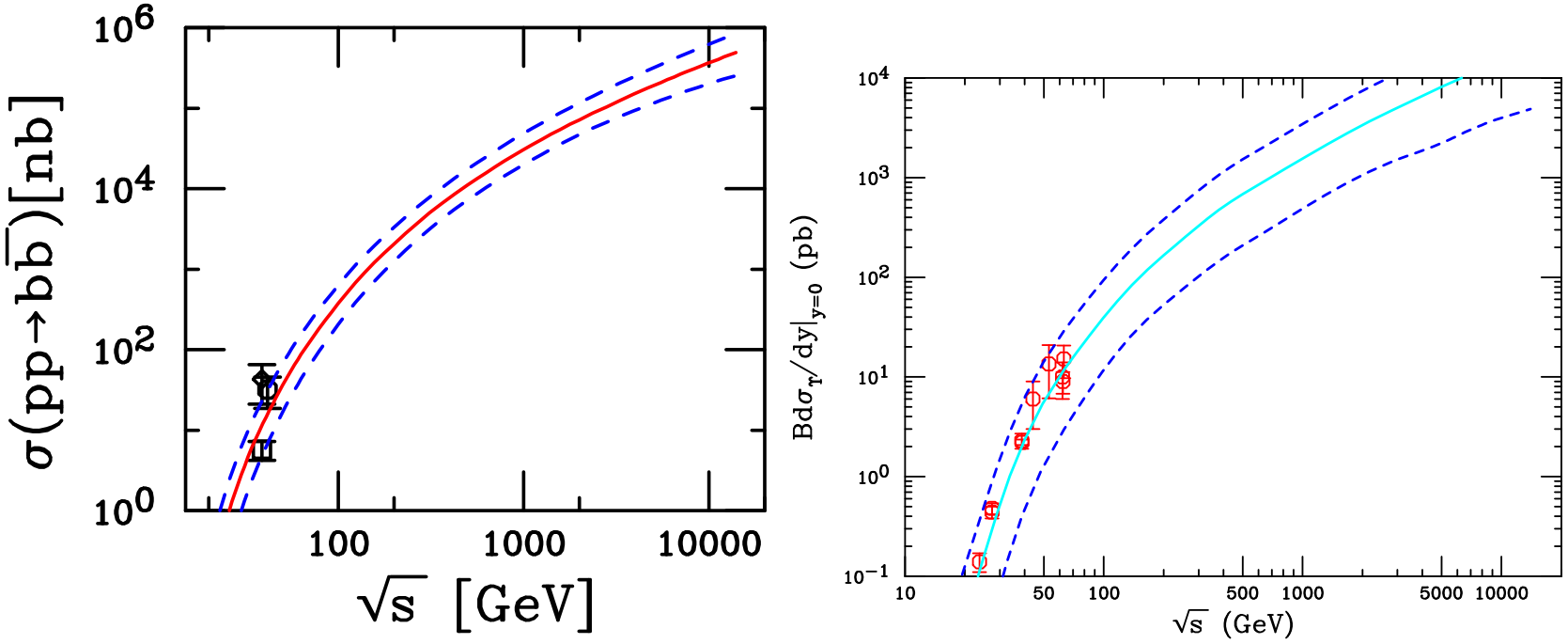

Figure 8: **The $b\bar{b}$ FONLL uncertainty band (left) and the combined Υ S states in the dilepton channel (right). Both are calculated to NLO in the CEM. [After Phys. Rept. 458 (2008) 1.]**

CEM Uncertainty Band for Υ

Wide uncertainty range in p_T distribution of Υ from FONLL choice of mass and scales

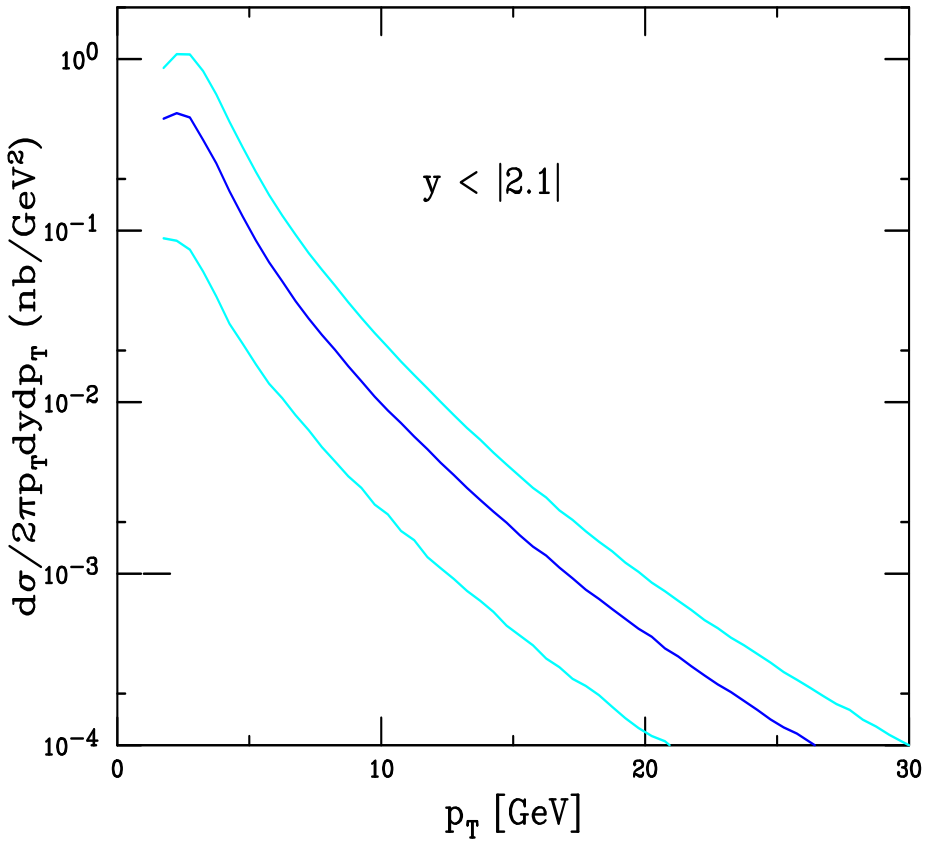

Figure 9: **The midrapidity Υ results using the FONLL uncertainty range. The blue curve is the central result while the cyan curves represent the upper and lower limits. The normalization is fixed for the central result.**

CEM p_T Distributions

Without intrinsic k_T smearing (or resummation) the $Q\overline{Q}$ p_T distribution (LO at $\mathcal{O}(\alpha_s^3)$ while total cross section is NLO at this order) is too peaked at $p_T \to 0$, needs broadening at low p_T

Implemented by Gaussian k_T smearing, $\langle k_T^2 \rangle_p = 1$ GeV^2 for fixed target pp and πp, broadened for pA and AA, NLO code adds in final state:

$$g_p(k_T) = \frac{1}{\pi \langle k_T^2 \rangle_p} \exp(-k_T^2/\langle k_T^2 \rangle_p)$$

Broadening should increase with energy we make a simple linear extrapolation to obtain

$$\langle k_T^2 \rangle_p = 1 + \frac{1}{3n} \ln\left(\frac{\sqrt{s}}{\sqrt{s_0}}\right) \text{ GeV}^2$$

We find $n \sim 4$ agrees best with RHIC data

Note that unlike FONLL-like calculation of single inclusive heavy flavor with resummed logs of p_T/m, at large p_T distribution may be harder than it should be

CEM Comparison to RHIC pp J/ψ Data

CEM calculation reproduces shape of J/ψ p_T and y distributions rather well considering that normalization is set from RHIC energies and below with only one parameter

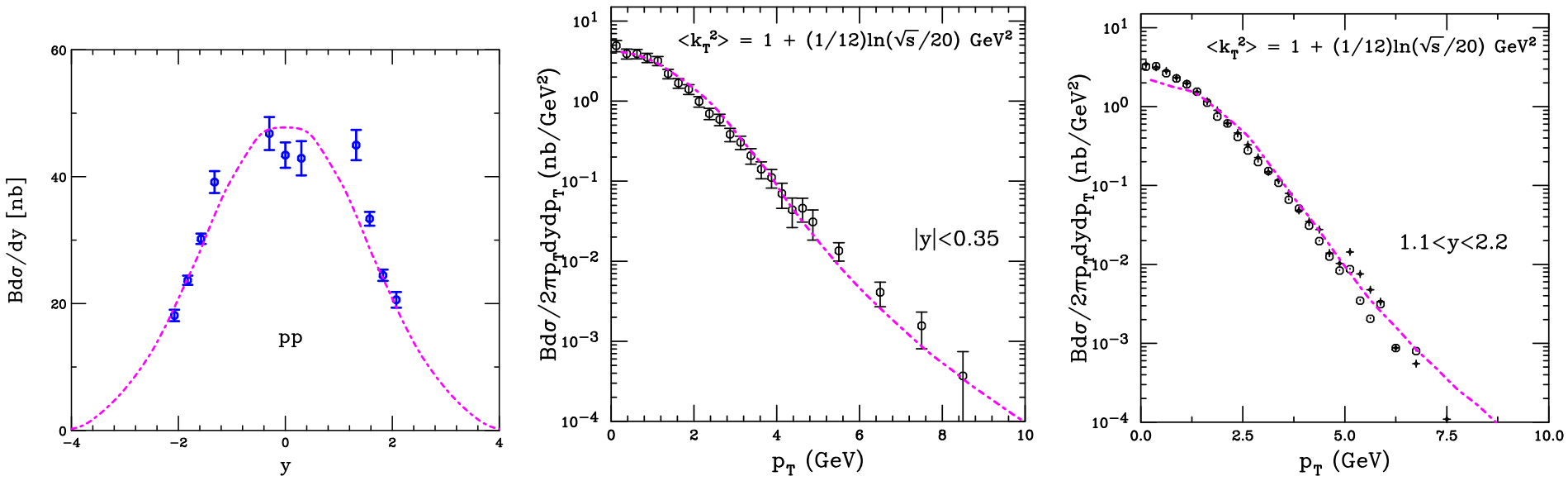

Figure 10: **PHENIX** pp **measurements compared to CEM calculation at** $\sqrt{s} = 200$ **GeV. The** J/ψ **rapidity distribution (left) and transverse momentum distributions at midrapidity (center) and in the muon arms (right). The results are calculated with CTEQ6M,** $(m, \mu_F/m_T, \mu_R/m_T) = (1.2, 2, 2)$**,** $\langle k_T^2 \rangle = 1.38$ **GeV**^{2}**. The forward result is scaled up by a factor of** ≈ 1.4**.**

CEM Comparison to Preliminary LHC pp Quarkonium Data

CEM calculation reproduces shape of J/ψ and $\Upsilon(1S)$ p_T distributions using CTEQ6M with $(m, \mu_F/m_T, \mu_R/m_T) = (1.2\ \text{GeV}, 2, 2)$, $\langle k_T^2 \rangle = 1.38$ GeV^2 and $(m, \mu_F/m_T, \mu_R/m_T) = (4.75\ \text{GeV}, 1, 1)$

No additional scale factor included

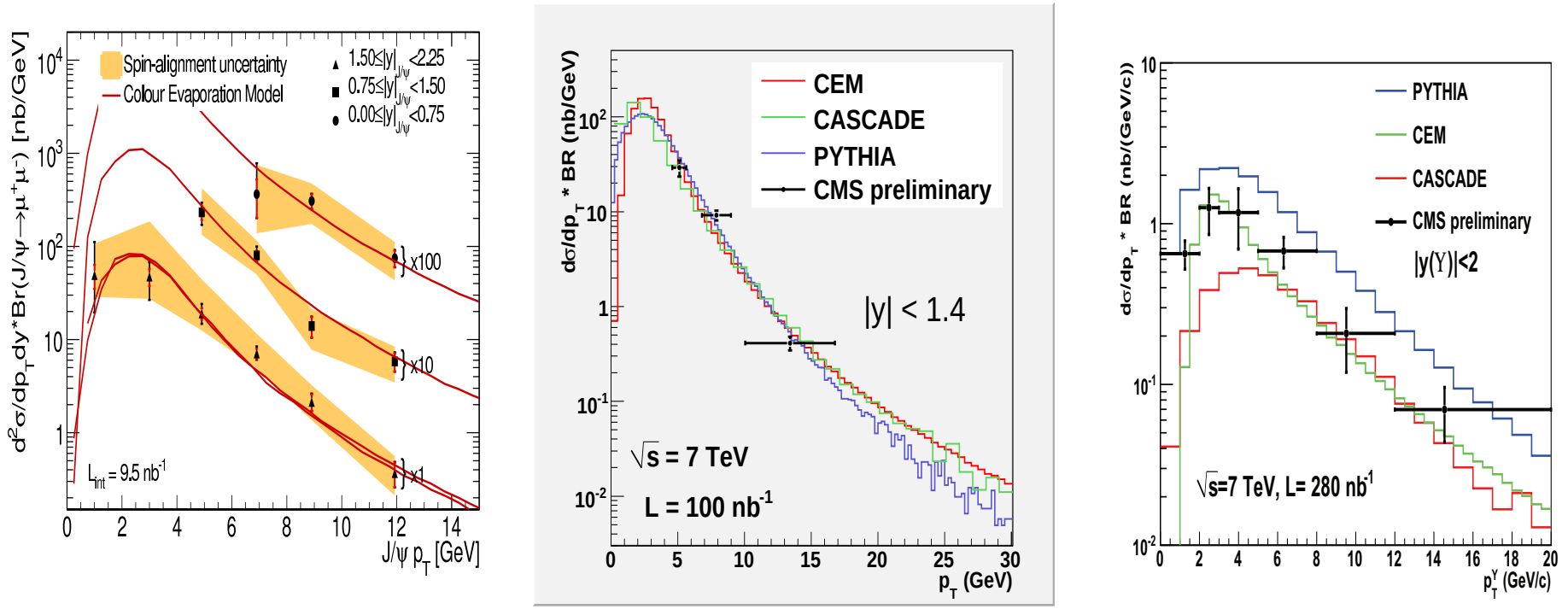

Figure 11: **ATLAS (left) and CMS (middle) J/ψ and CMS $\Upsilon(1S)$ (right) cross sections at 7 TeV compared to CEM calculations.**

CEM Uncertainty Using $c\bar{c}$ Fits

We show results both with $\mu_F = m_T$ and $2m_T$ even though $2m_T$ is clearly more consistent with overall energy dependence of cross section

For a given factorization scale curves have same slope, as expected
Normalization is fixed from individual fits

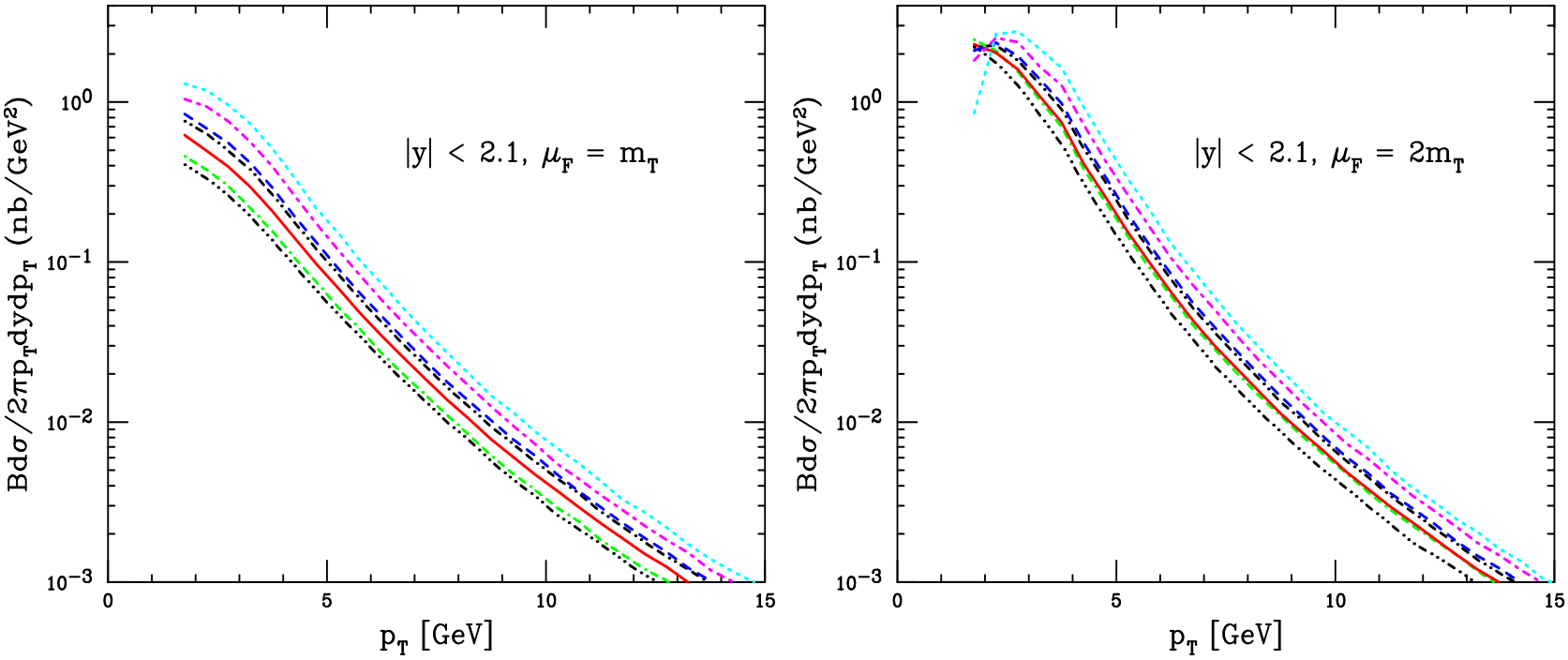

Figure 12: **The prompt J/ψ p_T distributions in the rapidity interval $|y| < 2.1$. The curves on the left-hand side are calculated with** $(1.1\,\text{GeV}, 1, 3.9)$ **[dot-dot-dot-dashed black],** $(1.15\,\text{GeV}, 1, 3)$ **[dot-dash-dash-dashed green],** $(1.2\,\text{GeV}, 2, 2.3)$ **[solid red],** $(1.27\,\text{GeV}, 1, 1.7)$ **[dot-dot-dash-dashed black],** $(1.3\,\text{GeV}, 1, 1.5)$ **[dashed blue],** $(1.4\,\text{GeV}, 1, 1)$ **[dot-dashed magenta], and** $(1.5\text{GeV}, 1, 0.8)$ **[dotted cyan] while those on the right-hand side are with** $(1.1\,\text{GeV}, 2, 4)$ **[dot-dot-dot-dashed black],** $(1.15\,\text{GeV}, 2, 3)$ **[dot-dash-dash-dashed green],** $(1.2\,\text{GeV}, 2, 2.2)$ **[solid red],** $(1.27\,\text{GeV}, 2, 1.6)$ **[dot-dot-dash-dashed black],** $(1.3\,\text{GeV}, 2, 1.4)$ **[dashed blue],** $(1.4\,\text{GeV}, 2, 1)$ **[dot-dashed magenta], and** $(1.5\text{GeV}, 2, 0.7)$ **[dotted cyan].** $(1.2\ \text{GeV}, 2, 2)$ **[solid red],** $(1.4\ \text{GeV}, 2, 1)$ **[dot-dashed magenta], and** $(1.5\ \text{GeV}, 2, 0.7)$ **[dotted cyan] using the CT10 PDFs. The curves are normalized by the forward cross section fits at fixed-target energy.**

Calculation of J/ψ Contribution from B decays

B production calculated using FONLL, uncertainty comes from varying the mass and scale around central value of $(4.75\,\mathrm{GeV}, 1, 1)$ and adding uncertainties in quadrature

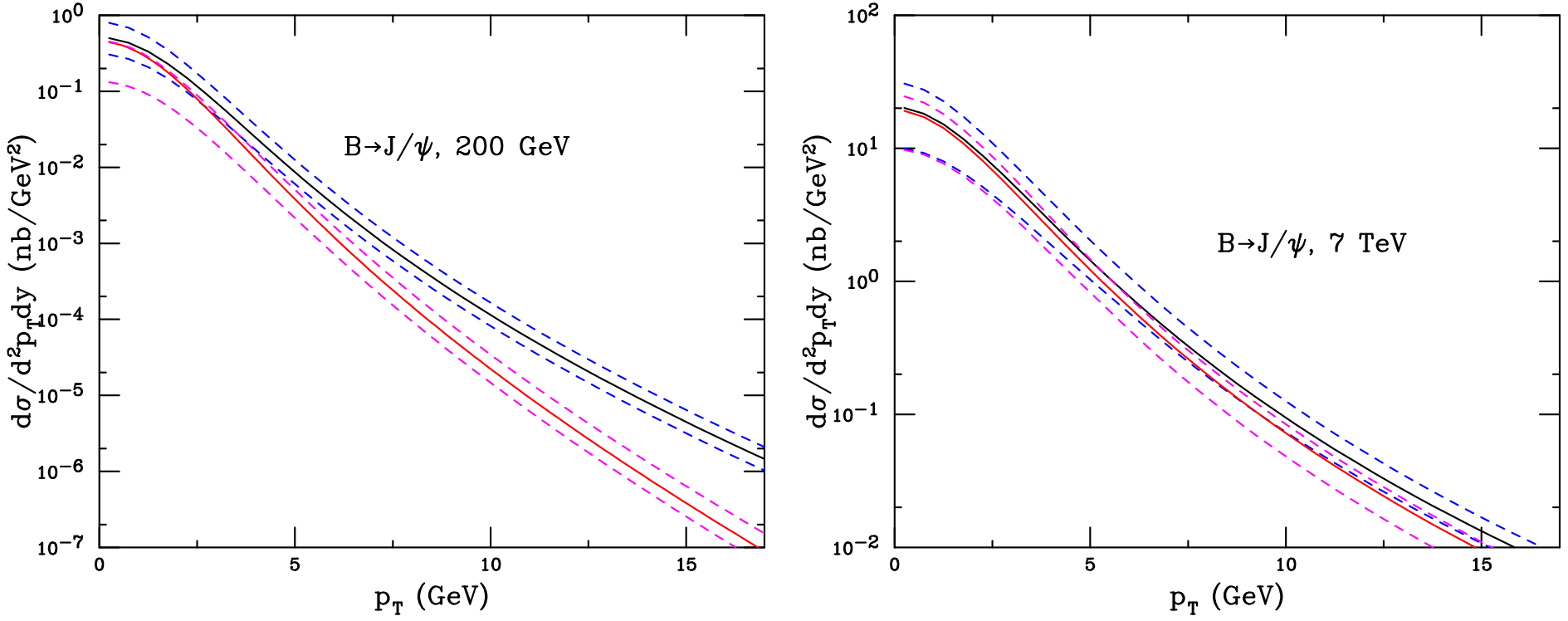

Figure 13: **Calculation of the invariant p_T distribution for B decay to J/ψ in pp collisions at $\sqrt{s} = 200$ GeV (left) and 7 TeV (right) from FONLL. The two rapidity bins for 200 GeV are $0.35 < |y|$ (black and blue) and $1.1 < |y| < 2.2$ (red and magenta) while the two bins for 7 TeV are $1.4 < |y|$ (black and blue) and $1.4 < |y| < 2.4$ (red and magenta).**

Fraction of J/ψ from B Decays at 200 GeV

$$B\,\text{fraction} \equiv \frac{B \to J/\psi X}{\text{prompt, inclusive}\, J/\psi + B \to J/\psi X}$$

Prompt inclusive J/ψ calculated in CEM with $(1.2\,\text{GeV}, 2, 2)$, band is from uncertainty on B cross section only, shape at high p_T depends on relative μ_F/m, μ_R/m values in prompt J/ψ calculation

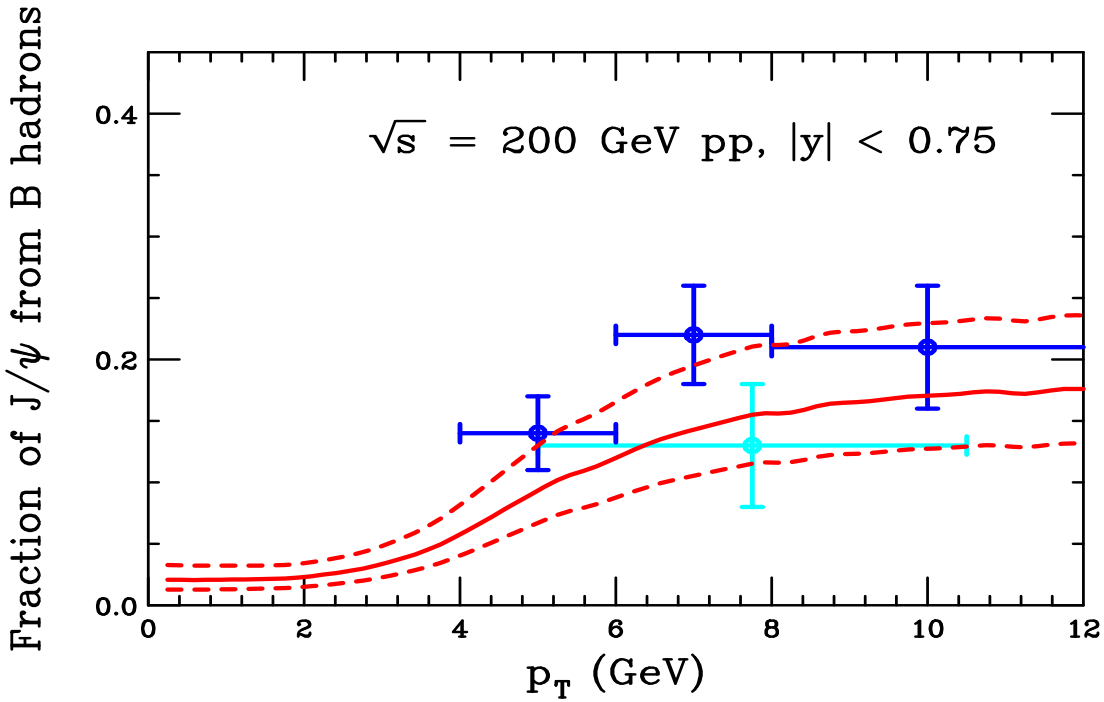

Figure 14: The fraction of J/ψ production from B decays as a function of p_T.

$B \to J/\psi$ Fraction at Tevatron and LHC

Good agreement with preliminary LHC pp data at 7 TeV

CDF $\overline{p}p$ data at 1.96 TeV has somewhat different curvature but only disagrees with calculated ratio for $p_T > 15$ GeV

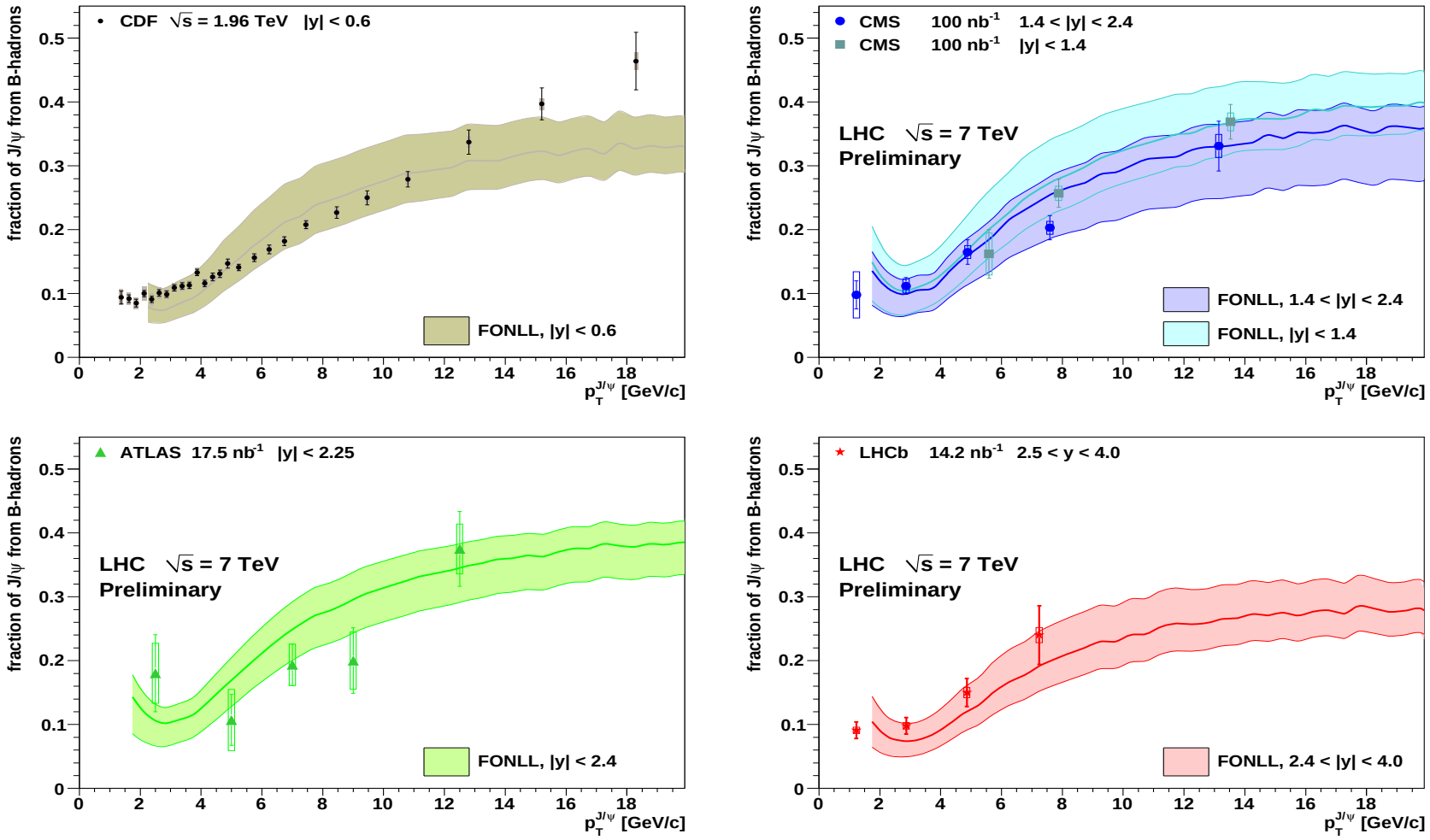

Figure 15: **The fraction of J/ψ from B decays at 1.96 TeV (CDF) and 7 TeV (CMS, ATLAS and LHCb).**

pA and dA Production

What Are Cold Matter Effects?

Important cold nuclear matter effects include:

- **Initial-state nuclear effects on the parton densities (shadowing)**
- **Initial-state energy loss**
- **Intrinsic heavy flavors**
- **Final-state absorption on nucleons**

Shadowing and absorption most important at midrapidity, initial-state energy loss and intrinsic heavy flavor more important at forward rapidity

Production mechanism affects both intimately:

- **Shadowing depends on momentum fraction x of the target (and projectile in AA) which is influenced by how the state was produced: $2 \to 1$ or $2 \to 2$ process**
- **Production affects absorption because singlet and octet states can be absorbed differently**

Comparing Shadowing Parameterizations

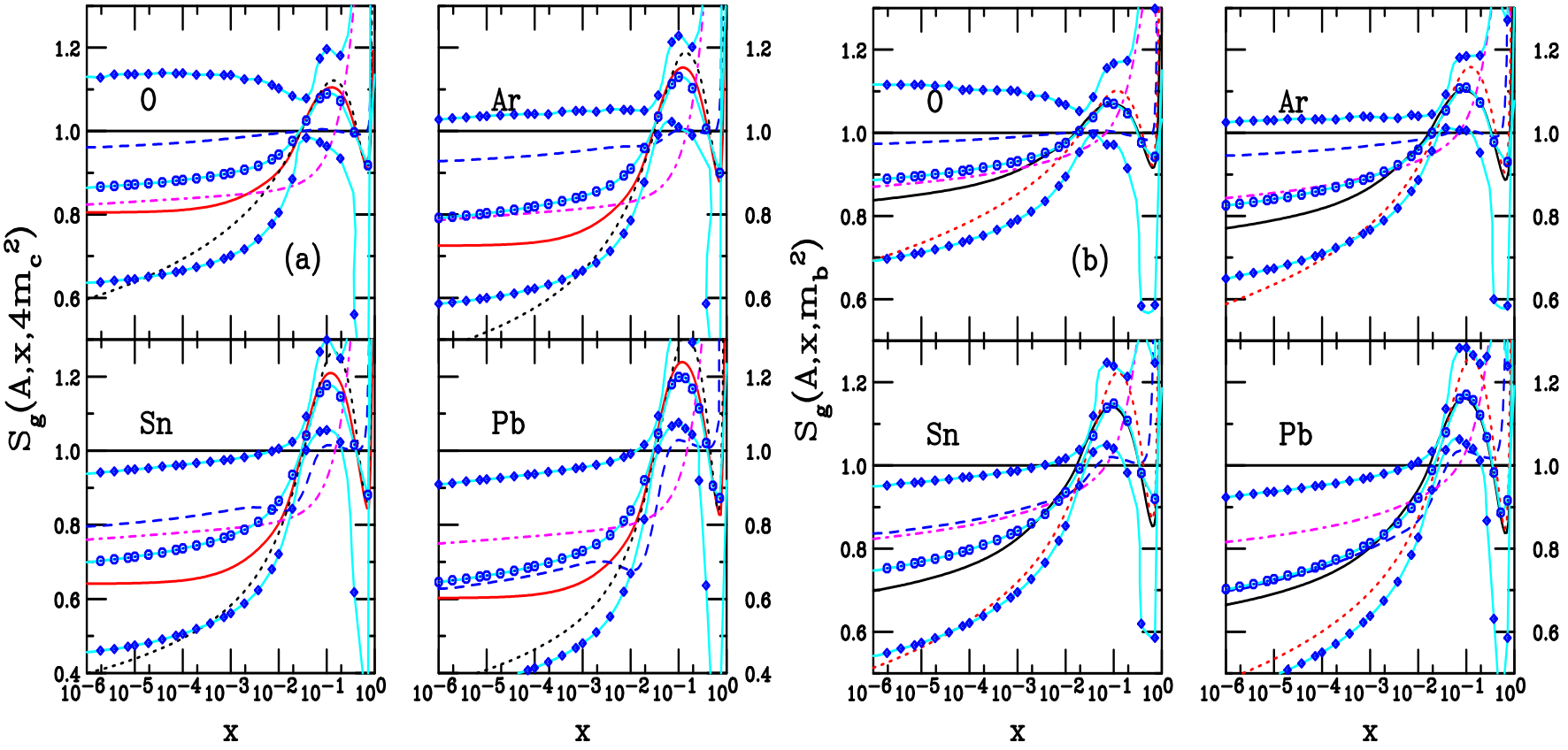

Figure 16: **Comparison of EKS98 (red), nDSg (blue), HKN (green), EPS08 (magenta), and EPS09 (cyan, with symbols) gluon shadowing parameterizations for J/ψ (left) and Υ (right) production scales with A =O, Ar, Sn and Pb.**

Effects of nPDFs at LO and NLO

While the magnitude of the absolute cross sections may differ at LO and NLO, the effect of shadowing is, by design, the same at LO and NLO

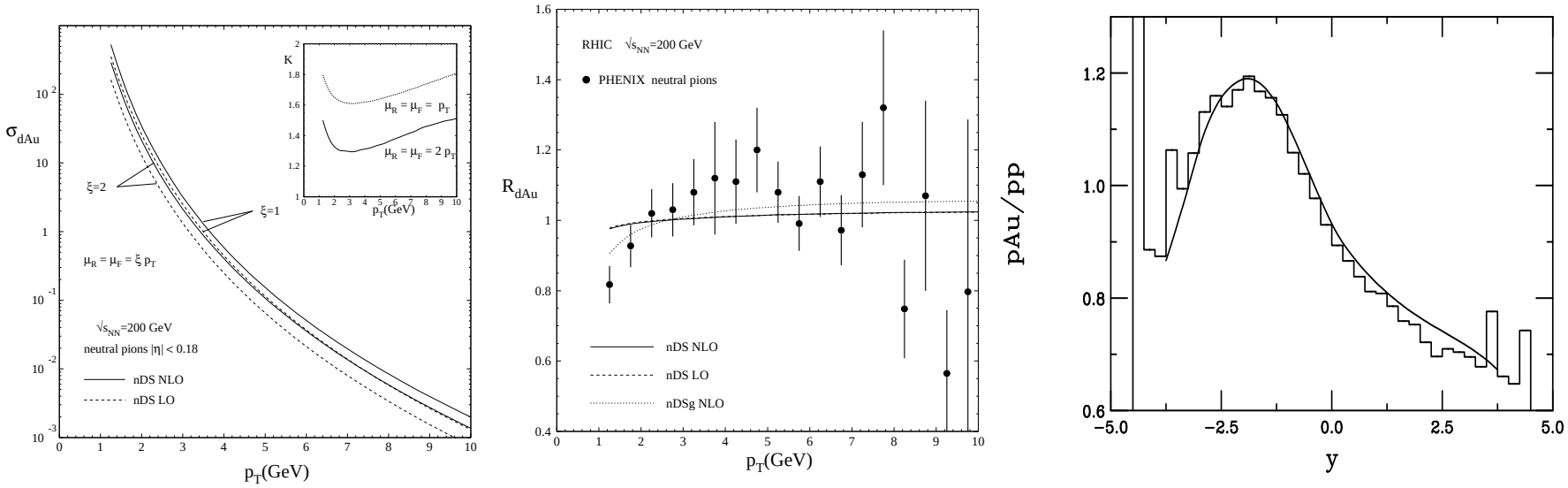

Figure 17: **Left: The π^0 cross section in d+Au collisions at $\sqrt{s_{NN}} = 200$ GeV at LO and NLO. Center: The LO and NLO calculations of $R_{\rm dAu}$ for π^0 production. Right: The J/ψ $R_{\rm dAu}$ as a function of rapidity at $\sqrt{s_{NN}} = 200$ GeV at LO (curve) and NLO (histogram).**

Quarkonium Absorption by Nucleons

Woods-Saxon nuclear density profiles typically used

$$\begin{aligned}\sigma_{pA} &= \sigma_{pN}\int d^2b \int_{-\infty}^{\infty} dz\, \rho_A(b,z) S_A^{\rm abs}(b) \\ &= \sigma_{pN}\int d^2b \int_{-\infty}^{\infty} dz\, \rho_A(b,z) \exp\left\{-\int_z^{\infty} dz' \rho_A(b,z')\sigma_{\rm abs}(z'-z)\right\}\end{aligned}$$

Note that if $\rho_A = \rho_0$, $\alpha = 1 - 9\sigma_{\rm abs}/(16\pi r_0^2)$

The value of $\sigma_{\rm abs}$ **depends on the parameterization of** σ_{pA} **– Glauber, hard sphere,** A^α **etc. (shown by NA50)**

Initial-state shadowing, only recently taken into account at SPS energies

Feed down to J/ψ **from** χ_c **and** ψ' **decays not always included, should dictate that**

$$\sigma_{pA} = \sigma_{pN}\int d^2b\, [0.6 S_{\psi,\,\rm dir}(b) + 0.3 S_{\chi_{cJ}}(b) + 0.1 S_{\psi'}(b)]$$

Assume that each charmonium state interacts with a different constant asymptotic absorption cross section

The χ_c A **dependence remains unknown**

Interplay of Shadowing and Absorption at SPS

Depending on x values probed, including shadowing can enhance or reduce absorption cross section needed to describe data

Stronger antishadowing of EKS98 in SPS midrapidity region calls for bigger absorption cross section

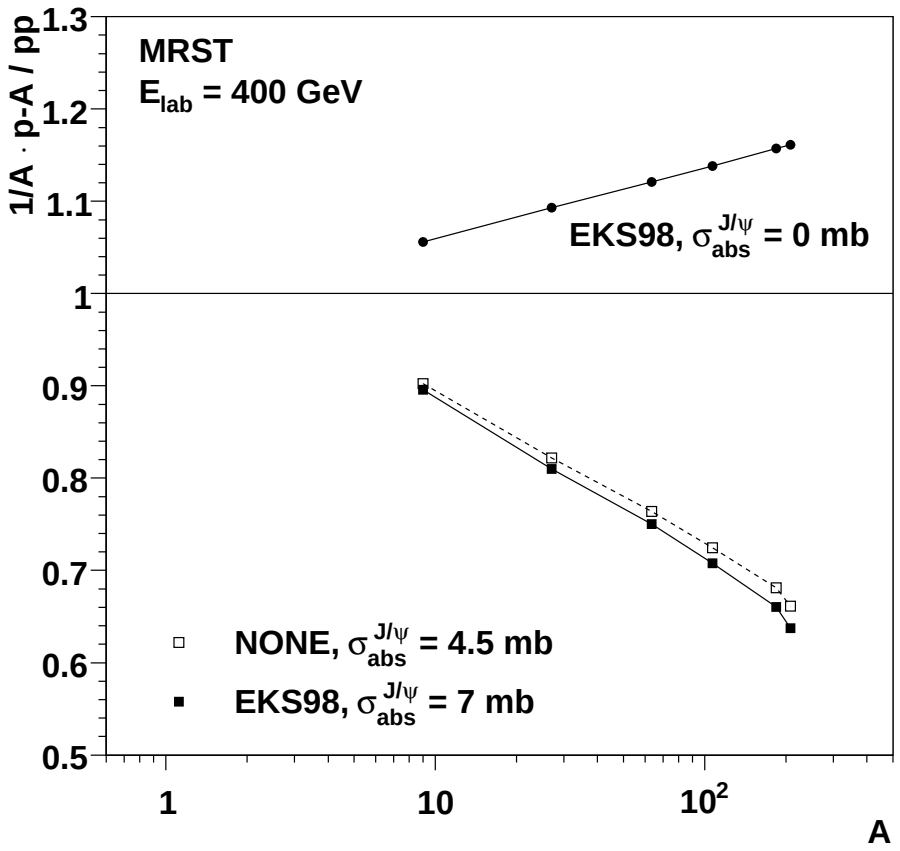

Figure 18: Illustration of the interplay between nuclear modifications of the parton densities and final-state charmonium absorption. [Lourenço, RV, Wöhri]

Energy Dependence of $\sigma_{\rm abs}^{J/\psi}$

At midrapidity, there seems to be a systematic decrease of the absorption cross section with energy independent of shadowing

$\sigma_{\rm abs}^{J/\psi}(y_{\rm cms}=0)$ extrapolated to 158 GeV is significantly larger than measured at 450 GeV, underestimating "normal nuclear absorption" in SPS heavy-ion data

Calculations confirmed by NA60 pA measurements at 158 GeV (QM09)

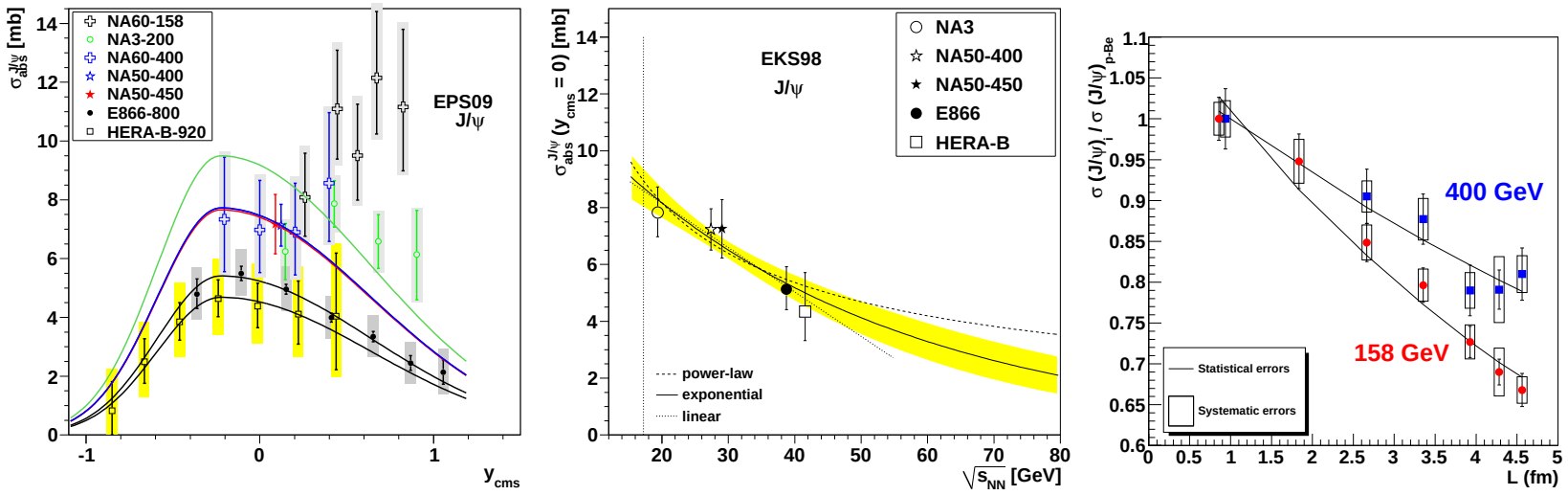

Figure 19: Left: Dependence of $\sigma_{\rm abs}^{J/\psi}$ on $y_{\rm cms}$ for all available data sets including EPS09 shadowing. The shape of the curves is fixed by the E866 and HERA-B data. [Lourenço, RV, Wöhri] Middle: The extracted energy dependence of $\sigma_{\rm abs}^{J/\psi}$ at midrapidity for power law (dashed), exponential (solid) and linear (dotted) approximations to $\sigma_{\rm abs}^{J/\psi}(y=0,\sqrt{s_{NN}})$ using the EKS98 shadowing parameterization with the CTEQ61L parton densities. The band around the exponential curve indicates the uncertainty in the extracted cross sections at $x_F \sim 0$ from NA3, NA50 at 400 and 450 GeV, E866 and HERA-B. The vertical dotted line indicates the energy of the Pb+Pb and In+In collisions at the CERN SPS. [Lourenço, RV, Wöhri] Right: The J/ψ cross section ratios for pA collisions at 158 GeV (circles) and 400 GeV (squares), as a function of L, the mean thickness of nuclear matter traversed by the J/ψ. [Arnaldi, Cortese, Scomparin]

Absorption Cross Section Negligible at LHC Energies?

Extrapolating our energy dependence, expect $\sigma_{\rm abs}^{J/\psi} << 1$ mb in pA collisions at LHC

Shadowing effects somewhat washed out with higher energy reference; rapidity shift flattens all ratios somewhat but ratios still different than no shadowing

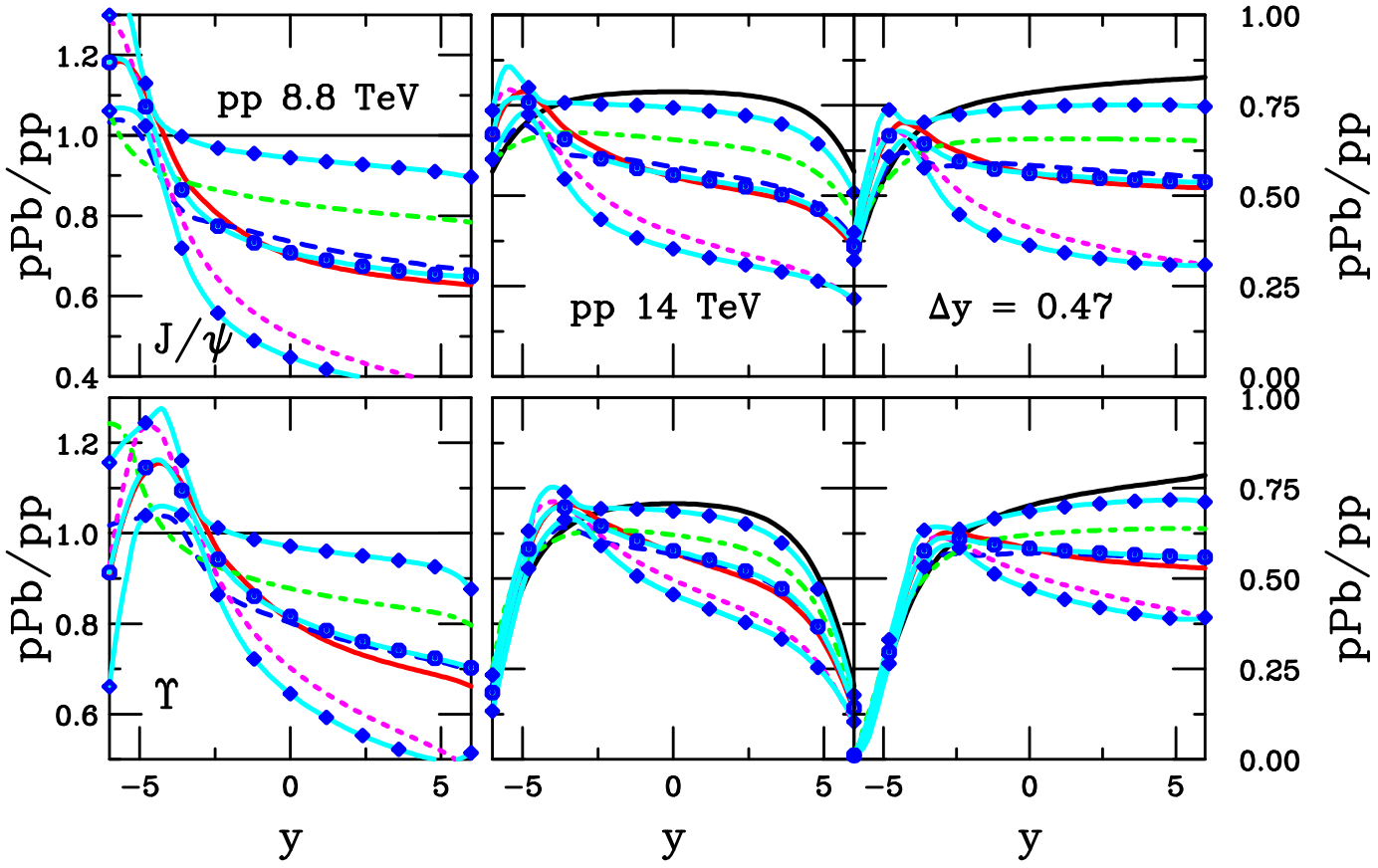

Figure 20: The pPb/pp ratios for J/ψ (top) and Υ (bottom) production at 8.8 TeV for: pA and pp collisions at the same center-of-mass energy and $\Delta y = 0$ (left); the pp reference at 14 TeV with $\Delta y = 0$ (center); and the higher energy pp reference and pA rapidity shift in the equal-speed frame taken into account (right). The curves show EKS98 (red solid), nDSg (blue dashed), HKN (green dot-dashed), EPS08 (magenta dotted) and EPS09 (cyan solid) shadowing parameterizations with no nuclear absorption. The black curves in the center and right panels show the ratios with no shadowing.

Etrapolating to AA Collisions

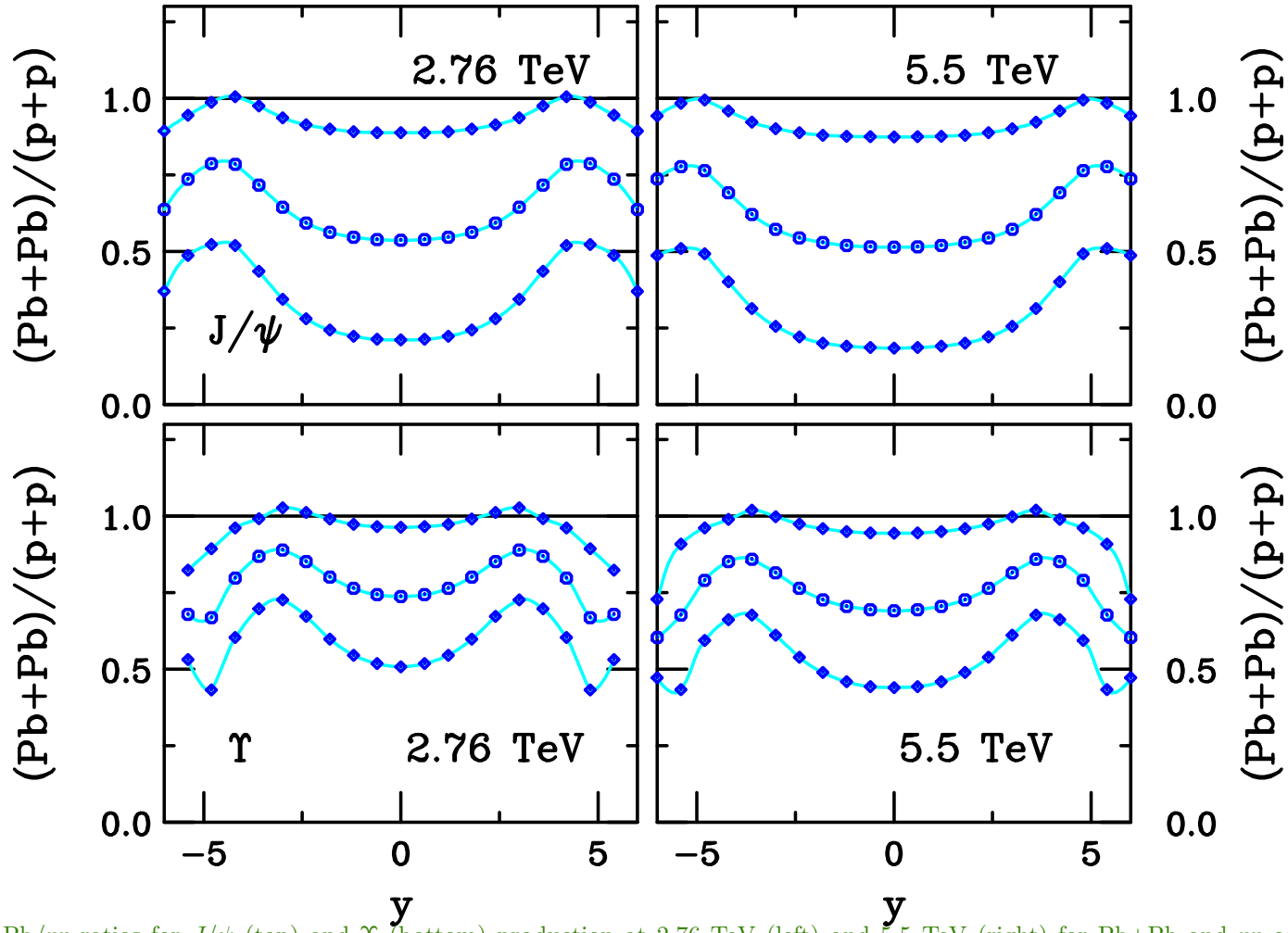

Figure 21: The PbPb/pp ratios for J/ψ (top) and Υ (bottom) production at 2.76 TeV (left) and 5.5 TeV (right) for Pb+Pb and pp collisions at the same center-of-mass energy. The curves show the EPS09 central set as well as the range of uncertainties with no absorption included.

$N_{\rm part}$ Behavior Assuming Linear Dependence of Shadowing on T_A

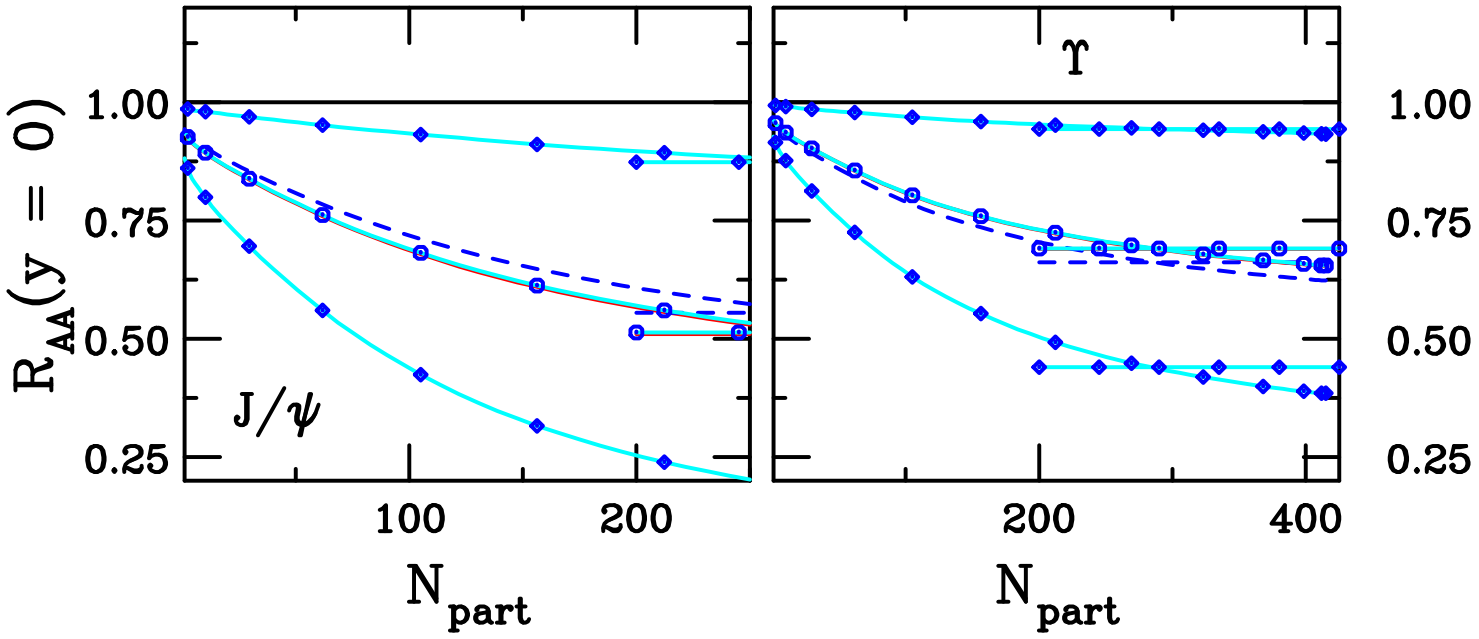

Figure 22: The PbPb/pp ratios for J/ψ (left) and Υ (right) at with Pb+Pb and pp collisions at 5.5 TeV and $y = 0$. The curves show the EPS09 central set as well as the range of uncertainties with no absorption included.

$\sigma_{\rm abs}^{J/\psi}(y_{\rm cms})$ Rises at Forward Rapidity

Forward x_F ($y_{\rm cms}$) data more complex: strongly increased absorption in this region

NA60 data begin to rise at lower x_F than do higher energy results from E866 and PHENIX R_{CP} data: CGC?!?, not low enough x

Such strong effects can't come from any shadowing parameterizations

Energy loss??? Or something else??? (See Tony's talk for more on PHENIX results and b dependence of shadowing.)

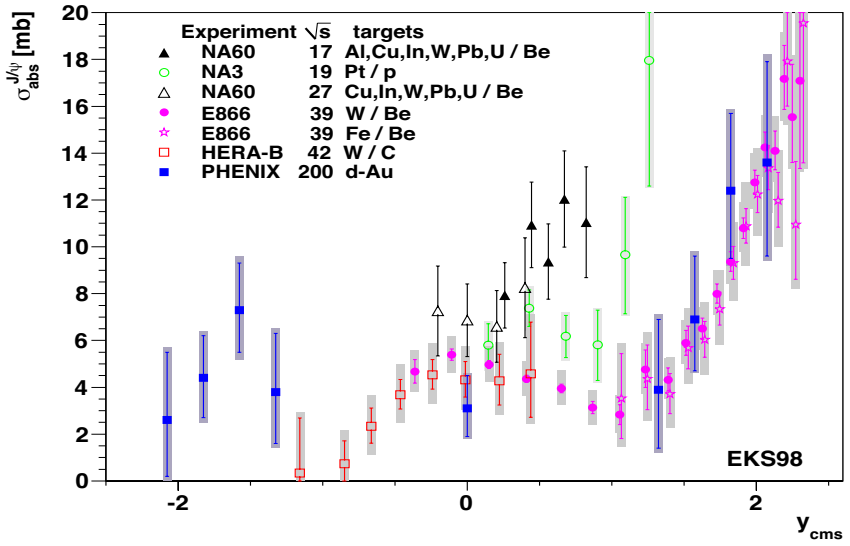

Figure 23: The center-of-mass rapidity dependence of $\sigma_{\rm abs}^{J/\psi}$ for incident fixed-target energies from 158, 200, 400, 450, 800, 920 GeV and preliminary PHENIX results from RHIC obtained using the EKS98 shadowing parameterization. (Plot made by Hermine Wöhri with PHENIX data from Tony Frawley.)

Drell-Yan Production: Testing Ground for Energy Loss

Good theory for pp production, small K factor with NLO calculation

$K = 1.124 \pm 0.007$, $\chi^2/\mathrm{ndf} = 1.4$ **relative to E866 measurements in 800 GeV pp collisions (J.C. Webb Ph.D. thesis [arXiv:hep-ex/0302019]).**

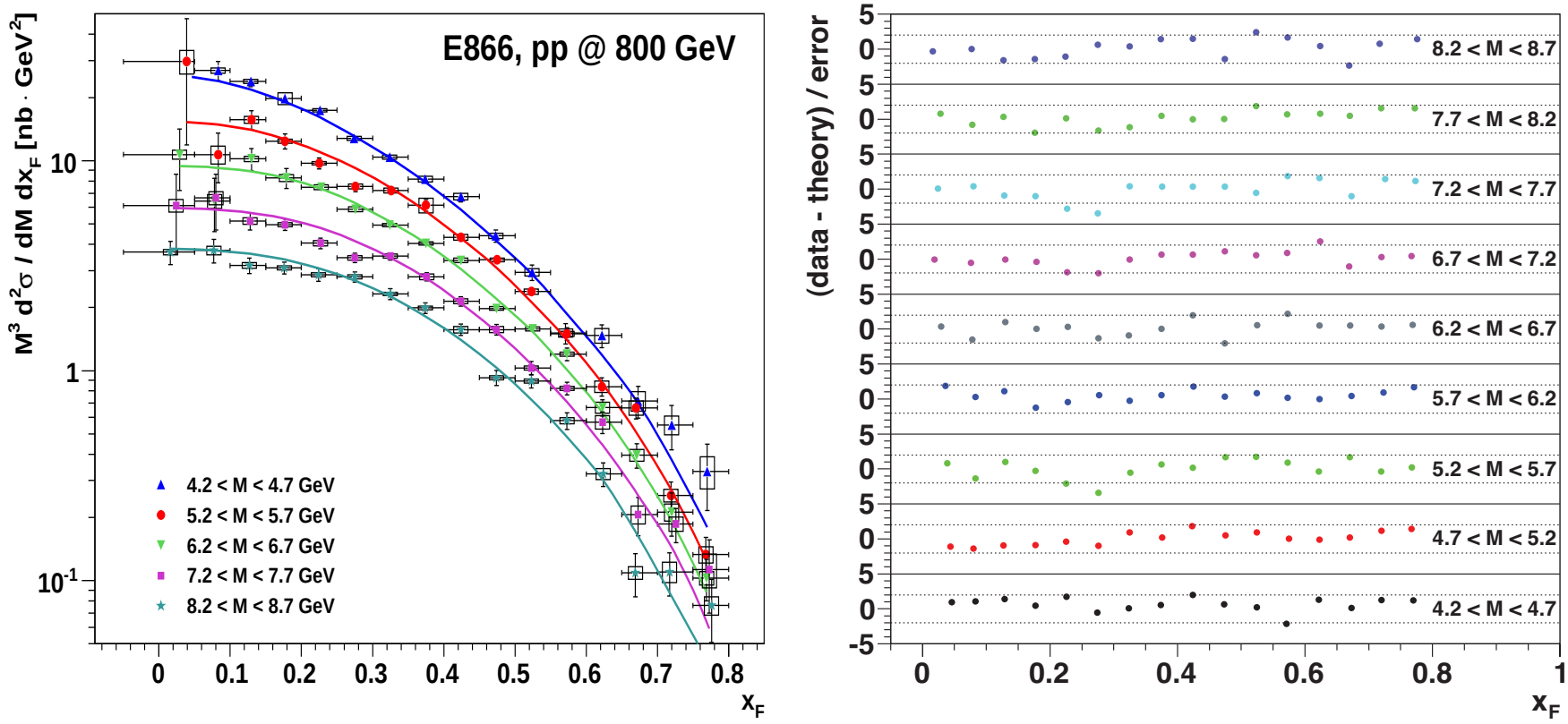

Figure 24: Left: The x_F dependence of the Drell-Yan cross section in several mass bins from 800 GeV pp colisions compared to NLO calculations. Right: Difference between the measured Drell-Yan cross section and the NLO calculations in the same mass bin.

Test Case: NA3 pPt Drell-Yan Production at 400 GeV

Compare NA3 data with NLO calculations with/without central EPS09 nPDFs (difference small)

Test parameterization of initial state energy loss

$$x_1' = x_1(1-\epsilon_q)^{N-1}$$

x_1' enters $M^2 = x_1' x_2 s_{NN}$, x_1 is in nPDFs, N is number of NN collisions, $\propto A^{1/3}$

Vary ϵ_q to get best fit, 99% confidence level gives upper limit on ϵ_q of 0.0020

Assume $\epsilon_g = (9/4)\epsilon_q$ for NLO qg contribution

$K \sim 1$, χ^2/ndf slightly smaller with no shadowing

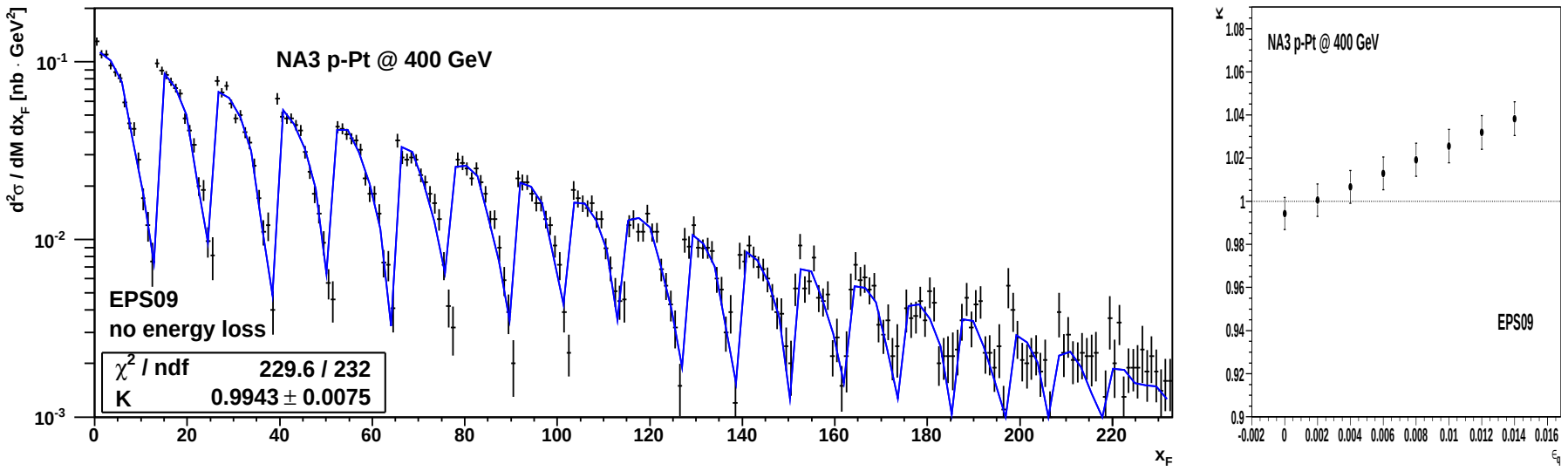

Figure 25: Left: The invariant DY cross section in pPt collisions at 400 GeV as a function of x_F in different mass bins with EPS09 nPDFs. Right: The K factors found in comparison to the data with various values of the energy loss parameter ϵ_q.

Adding Initial State Energy Loss to J/ψ Production

Rather large EPS09 uncertainty reduced in ratios; clearly initial-state shadowing is insufficient to describe effect

Combination of shadowing and energy loss with relatively x_F-independent absorption compares relatively well with the data for $x_F > 0.2$; HOWEVER, the assumed ϵ_q is much larger than found for Drell-Yan production

Stronger absorption closer to target? Formation time effects not yet included

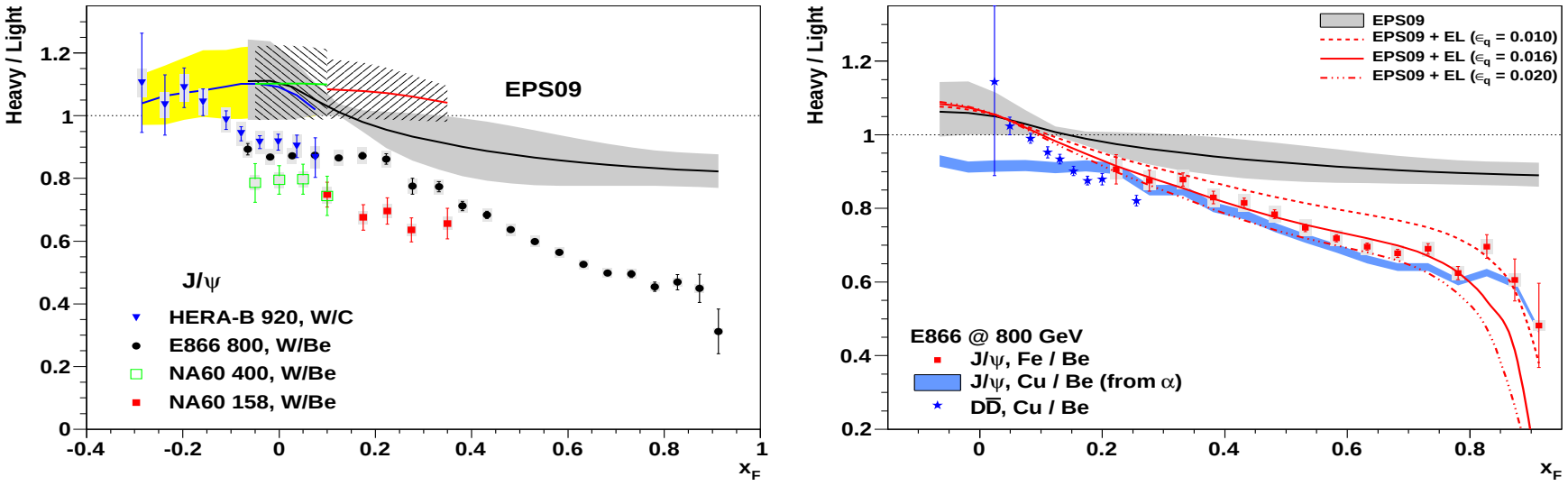

Figure 26: Left: The heavy to light ratios for W/Be in fixed target interactions. Right: Convolution of shadowing, absorption and various strengths of initial-state energy loss by quarks compared to the E866 data.

Summary .

- **Original version of CEM with exclusive NLO $Q\overline{Q}$ calculation does well against production data, especially considering that it has only one parameter to fix**
- **Preliminary attempt to place some uncertainty on J/ψ and Υ results, in progress**
- **Data seem to suggest absorption cross section decreases with $\sqrt{s_{NN}}$ and increases at forward x_F, obviously effects still unaccounted for, work in progress**
- **Study well-understood Drell-Yan production to get a handle on energy loss mechanism .**

A Dependence of J/ψ and ψ' Not Identical: Size Matters

Color octet mechanism suggested that J/ψ and ψ' A dependence should be identical — supported by large uncertainties of early data

More extensive data sets (NA50 at SPS, E866 at FNAL) show clear difference at midrapidity [NA50 ρL fit gives $\Delta\sigma = \sigma^{\psi'}_{\rm abs} - \sigma^{J/\psi}_{\rm abs} = 4.2 \pm 1.0$ mb at 400 GeV, 2.8 ± 0.5 mb at 450 GeV for absolute cross sections]

Suggests we need to include relative sizes and/or formation time effects

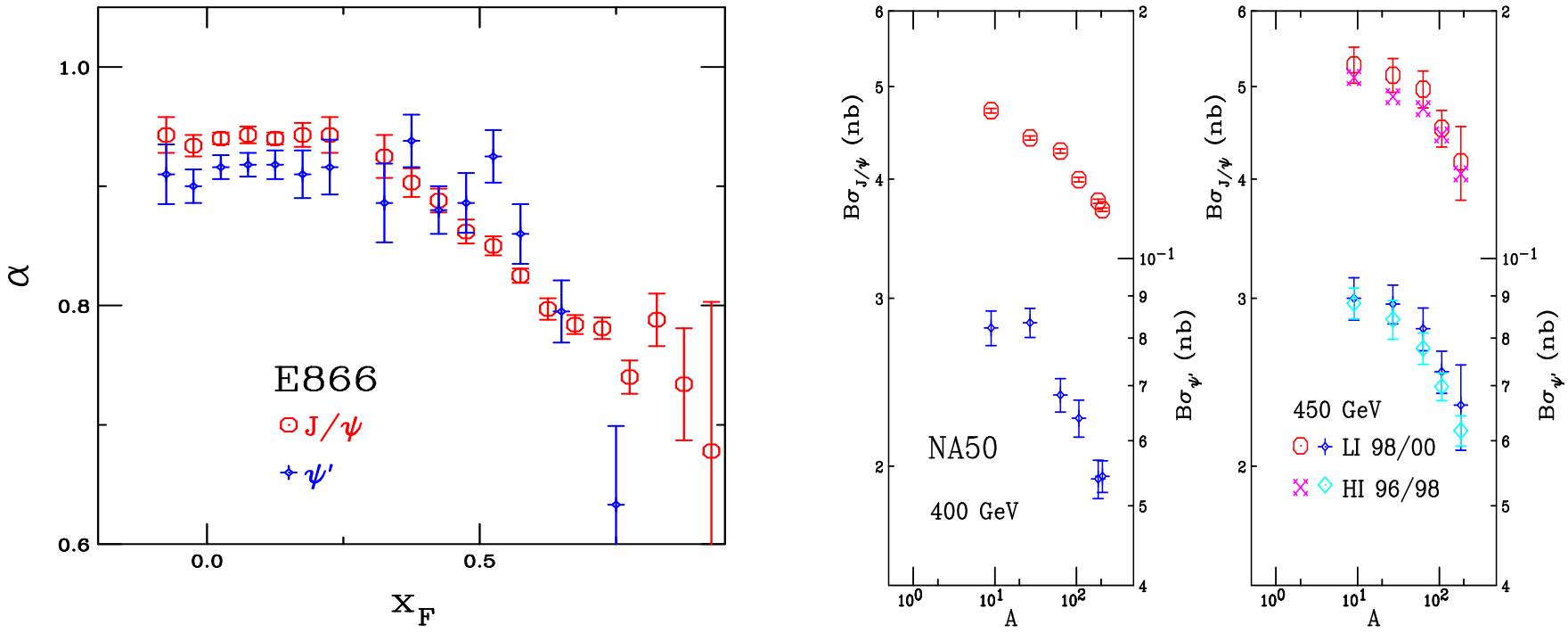

Figure 27: **The J/ψ A dependence (left) as a function of x_F at FNAL ($\sqrt{s_{NN}} = 38.8$ GeV) and (right) and a function of A at the SPS (NA50 at $p_{\rm lab} = 400$ and 450 GeV) for J/ψ and ψ' production.**

Nuclear Parton Distributions

Nuclear parton densities

$$\begin{aligned} F_i^A(x,Q^2,\vec{r},z) &= \rho_A(s) S^i(A,x,Q^2,\vec{r},z) f_i^N(x,Q^2) \\ s &= \sqrt{r^2+z^2} \\ \rho_A(s) &= \rho_0 \frac{1+\omega(s/R_A)^2}{1+\exp[(s-R_A)/d]} \end{aligned}$$

With no nuclear modifications, $S^i(A,x,Q^2,\vec{r},z) \equiv 1$

Assume spatial dependence proportional to a power of nuclear path length:

$$S^i_\rho(A,x,Q^2,\vec{r},z) = 1 + N_\rho(S^i(A,x,Q^2)-1)\Big(\frac{\int dz \rho_A(\vec{r},z)}{\int dz \rho_A(0,z)}\Big)^n$$

Alternatively, assume spatial dependence proportional to power of nuclear density:

$$S^i_{\rm WS}(A,x,Q^2,\vec{r},z) = 1 + N_{\rm WS}(S^i(A,x,Q^2)-1)\Big(\frac{\rho_A(\vec{r},z)}{\rho_A(0,z)}\Big)^n$$

Density-dependent parameteriation has sharper transition from shadowing to no shadowing as a function of impact parameter

Deutron density uses Hulthen wavefunction to calculate density

Normalization: $(1/A)\int d^2r dz \rho_A(s) S^i_\rho \equiv S^i$**. Larger than average modifications for** $s=0$**. Nucleons like free protons when** $s \gg R_A$**.**

Changing Impact Parameter Dependence of Shadowing

Assuming normal deuteron density with path length dependence gives rather slow change with b, increasing the power of the path length increases the central value and makes $S_{\mathrm{d}A}(b) \to 1$ faster

Assuming path length dependence with pA interactions instead of dA (only one nucleon in deuteron interacts) deepens and sharpens b dependence

Assuming density dependence in pA does not deepen density dependence as much but $S_{pA} \to 1$ at higher b

All results shown for $y = 2$, similar at other rapidities

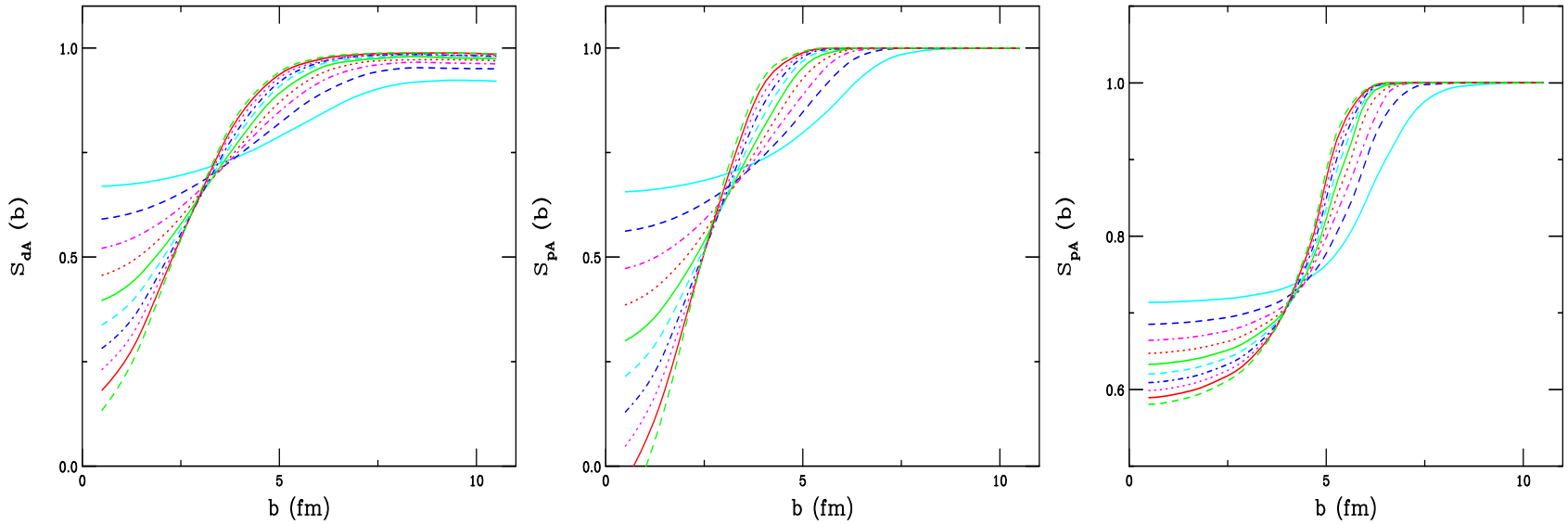

Figure 28: Changing the power of shadowing b-dependence from $n = 1$ (solid cyan) to 10 (dashed green) for dA collisions (left) and pA collisions (middle) with the path-length dependence and pA collisions with local density dependence (right). All calculations are at $y = 2$.